# Cytotoxic effect of Ruthenium-Arene Complexes containing tetrazolo[1,5-a] quinoline derivatives on cervical (HeLa), lung (A549), and colon (HCT116) cancer cell lines.

**S. Navitha[a], A. S. W. Wilfred Raj[b], S. Sree Brindha[a], M. Ravi[b*], F. Dallemer[c], G. Prabusankar[d] and R. Prabhakaran[a*]**

[a]Department of Chemistry, Bharathiar University, Coimbatore, 641 046, India.
[b]Department of Biochemistry, University of Madras, Guindy Campus, Chennai, 600025, India.
[c]Lab MADIREL CNRS UMR 7246, Aix Marseille University, Saint-Jerome Campus, MADIREL Bldg., 13397 Marseille Cedex 20, France.
[d]Department of Chemistry, Indian Institute of Technology, Hyderabad 502285, India.
*Corresponding author's E-mail:rpnchemist@gmail.com; rpnchemist@buc.edu.in
*Corresponding author's E-mail:ravimano2004@gmail.com

## Supplementary Information

## Materials and methods

All the reagents and starting ancestors used were of analytically and chemically pure grade and the solvents were dried according to the literature procedure.[1] Tetrazolo [1,5-a] quinoline-4-carboxaldehyde and 4-(hydrazonomethyl)tetrazolo[1,5-a] quinoline was synthesized according to the literature procedure.[2,3] Melting points were determined on Raaga apparatus. Infrared spectra were recorded in the range of 400-4000 $cm^{-1}$ (KBr pellets) on a Jasco FT-IR spectrometer. Electronic absorption spectra of the compounds were recorded using JASCO 600 spectrophotometer and emission measurements were carried out by using DMSO on a JASCO FP-6600 spectrofluorometer. $^{1}H$ and $^{13}C$-NMR spectra of the compounds were recorded at room temperature in DMSO-$d_6$ and $CDCl_3$ by using a Bruker 400 MHz instrument. Chemical shifts (δ) were presented in parts per million with reference to the signal of tetramethylsilane (TMS). Single crystal data collections and corrections for the ligands (**AQHS[1-3]**) and complexes **C1-C4** were done with CCD plate Kappa Diffractometer using graphite monochromator with Mo Kα radiation (λ = 1.54184 Å and 0.71073 Å) radiation. Data reduction was performed using CrysAlisPro software (version 1.171.42.49) developed by Rigaku Oxford Diffraction. The structural solution was done by using SHELXT 2018/2 (Sheldrick, 2018) and refined by full matrix least square on $F^2$using SHELXL-2018/3 (Sheldrick, 2015). The electrochemical behaviour of the synthesized ligands and ruthenium(II) complexes (1mM) was studied using acetonitrile as solvent with a sweep range ±2.00 V at a scan rate of 100 mV $s^{-1}$ by using platinum wire working electrode, platinum disc counter electrode and all the potentials were referenced to non-aqueous Ag/AgCl electrode. 0.1 M tetrabutylammonium perchlorate was

used as supporting electrolyte. Circular dichroism (CD) spectra of CT–DNA (10 μM) were recorded in JASCO J-1500 using Tris-HCl buffer, both in the absence and in the presence of ruthenium(II) complexes C1-C4 (10μM). Each sample was scanned over the wavelength range of 200–320 nm at a scan rate of 100 nm $min^{-1}$. CT-DNA, BSA and ethidium bromide (EB) were obtained from Hi-media.

**DNA binding experiment**

In all experiments involving the binding of the complexes to Calf Thymus DNA (CT-DNA), a buffer solution was prepared by dissolving tris(hydroxymethyl)aminomethane (5 mM) and sodium chloride (50 mM) in deionised water. The pH of the solution was adjusted to 7.2 at room temperature using hydrochloric acid. Solutions of CT-DNA in Tris-HCl buffer gave a ratio of UV absorbance at 260 and 280 nm, $A_{260}/A_{280}$, of approximately 1.9, indicating that the DNA was sufficiently free of protein. The concentration of CT-DNA was determined by UV absorbance at 260 nm. The molar absorption coefficient, $\varepsilon_{260}$, was taken as 6600 $M^{-1}$ $cm^{-1}$. Various concentrations of CT-DNA (0-10 μM) was added to the ligands and complexes (10 μM dissolved in a DMSO/TrisHCl buffer, 1 % DMSO in the final solution). While measuring the absorption spectra, an equal amount of DNA was added to both the test solution and the reference solution to eliminate the absorbance of DNA itself. Control experiments with DMSO were performed and no changes in the spectra of CT-DNA were observed. Absorption spectra were recorded after equilibrium at 20° C for 10 min. The intrinsic binding constant $K_b$ was determined by using following equation (S1)

$$[DNA]/[\varepsilon_a-\varepsilon_f]) = [DNA]/[\varepsilon_b-\varepsilon_f]+1/K_b[\varepsilon_b-\varepsilon_f] \quad (S1)$$

The absorption coefficients $\varepsilon_a$, $\varepsilon_f$ and $\varepsilon_b$ correspond to $A_{obsd}/[DNA]$, the extinction coefficient for the free compound and the extinction coefficient for the compound in the fully bound form respectively. The slope and the intercept of the linear fit of the plot of $[DNA]/[\varepsilon_a-\varepsilon_f]$ versus [DNA] give $1/[\varepsilon_a-\varepsilon_f]$ and$1/K_b[\varepsilon_b-\varepsilon_f]$, respectively. The intrinsic binding constant $K_b$ can be obtained from the ratio of the slope to the intercept.[4] In order to find out the mode of attachment of CT DNA to the compounds, fluorescence quenching experiments of EB-DNA were carried out by adding our complexes to the Tris-HCl buffer of EB-DNA. The change in the fluorescence intensity was recorded. Before measurements, the system was shaken well and incubated at room temperature for 5 min. The emission was recorded at 550–750 nm.[5]

**Serum albumin binding study**

The protein binding study was performed by tryptophan fluorescence quenching experiments using bovine serum albumin (BSA, 10 μM) as the substrate in phosphate buffer (pH= 7.4). Quenching of the emission intensity of tryptophan residues of BSA at 350 nm (excitation wavelength at 280 nm) was monitored using ligands and complexes as quenchers with increasing concentration (10-100 μM). Synchronous fluorescence spectra of BSA with various concentrations of the complexes were obtained from 300 to 400 nm when $\Delta\lambda$ = 60 nm and from 290 to 500 nm when $\Delta\lambda$ = 15 nm. For synchronous fluorescence spectra, the same concentrations of serum albumins and the compounds were also used and the spectra were measured at two different $\Delta\lambda$ values (difference between the excitation and emission wavelengths of BSA), such as 15 and 60 nm. Fluorescence and synchronous measurements were performed using a 1 cm quartz cell on a JASCO FP 6600 spectrofluorimeter.[8]

The quenching data can be analysed according to the Stern-Volmer equation,

$$I_o/I_{corr} = K_{SV}[Q]+1 \qquad \text{Eq. (S2)}$$

where $I_o$ is the emission intensity in the absence of compound, $I_{scor}$ is the corrected emission intensity in the presence of compound, $K_{SV}$ is the quenching constant and [Q] is the concentration of the compound.

In order to correct the inner filter effect, the following equation used

$$I_{corr} = I_{obs} * 10^{(Aexc+Aem)/2}$$

where, $I_{scor}$ is the corrected fluorescence value, $I_{obs}$ the measured fluorescence value, $A_{exc}$ is the absorption value at the excitation wavelength, and $A_{em}$ the absorption value at the emission wavelength.

The equilibrium binding constant and the number of binding sites can be analyzed by using Scatchard equation

$$\log [(F_o-F)/F] = \log K_b + n \log [Q] \quad \text{Eq. (S3)}$$

where, $F_o$ and F are the corrected emission intensities of serum albumins in the absence and presence of the compounds, where n is the binding site per albumin and $K_b$ is the binding constant.[9]

**Cell Culture**

HeLa, A549, HCT116, and L132 cells were obtained from the National Centre for Cell Science (NCCS), Pune. The cells were cultured in Dulbecco's Modified Eagle Medium (DMEM) supplemented with 10% fetal bovine serum (FBS) and 1% penicillin/streptomycin. Once the cells reached 70–80% confluence, the medium was removed, and the cells were rinsed with 1 mL of 1× phosphate-buffered saline (PBS). Subsequently, 1 mL of trypsin-EDTA solution was added

to detach the cells. The cell suspension was then centrifuged, and the pellet was re-suspended in fresh complete medium, transferred to sterile culture plates, and used for further experiments.

**Cell Viability Assay**

Indicated cells were seeded in 96-well plates at a density of 1 x $10^4$ cells per well and incubated overnight. Ruthenium complexes (**C1**–**C4**), along with *cisplatin* as a reference drug, were applied in a dose-dependent manner (25–100 μM) and incubated for 48 hours. After incubation, 5 mg/mL of MTT reagent was added to each well and incubated for an additional 2–4 hours in the dark. The medium was then discarded, and the resulting formazan crystals were dissolved in DMSO. Absorbance was measured at 570 nm using a microplate reader. $IC_{50}$ values were calculated using GraphPad Prism 8 software.[7]

**Cell morphology assay**

HeLa and A549 cells were seeded in 6-well plates at a density of 5 x $10^4$ cells per well and treated with **C4** for 48 hours. Post-treatment, the cells were washed with 1× PBS, and morphological changes were observed under an inverted microscope (Zenoptik-GRYPHAX).[6,7]

**Fluorescence microscopy assay**

HeLa and A549 cells were seeded on sterile coverslips placed in 6-well plates at a density of 5 x $10^4$ cells/well and incubated for 24 hours. The cells were then treated with **C4** for 48 hours. After treatment, the medium was removed, and cells were washed with 1× PBS. Staining was performed using acridine orange (AO) and ethidium bromide (EtBr) (1 mg/mL, mixed in a 1:1 ratio). The stained coverslips were mounted onto glass slides, and fluorescence images were captured using an inverted fluorescence microscope at an emission range of 525–605 nm.[6]

**Wound Healing Assay**

HeLa and A549 cells were seeded in 6-well plates at a density of 5 x $10^4$ cells/well and allowed to grow to confluence over 24 hours. A linear wound was created in the monolayer using a sterile 200 μL pipette tip. The cells were then treated with **C4**. Images of the wound area were captured at 0, 24, and 48 hours using an inverted microscope to assess cell migration.[8,9]

**Migration Assay**

HeLa and A549 cells (5 x $10^4$ cells) were seeded into the upper chamber of a Transwell insert placed in a 6-well plate and treated with **C4** for 48 hours. After incubation, non-migrated cells were removed, and the migrated cells on the lower surface were fixed with 200 μL of 4% paraformaldehyde at –20°C for 1 hour. The cells were then stained with 0.5% crystal violet, washed with 1× PBS, and visualized under an inverted microscope.[8,9]

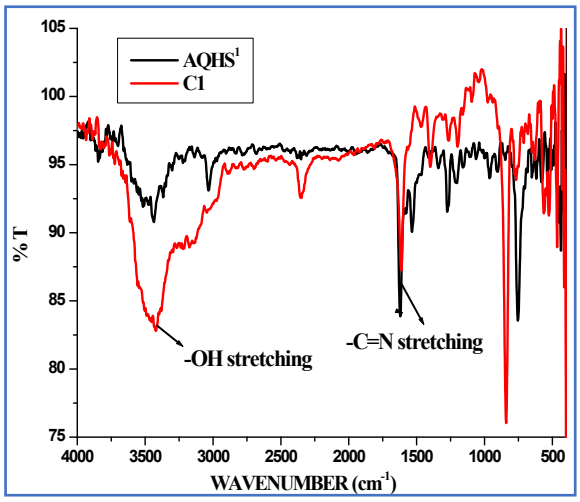


**Fig. S1.** IR spectra of ligand **AQHS[1]** and complex**C1**

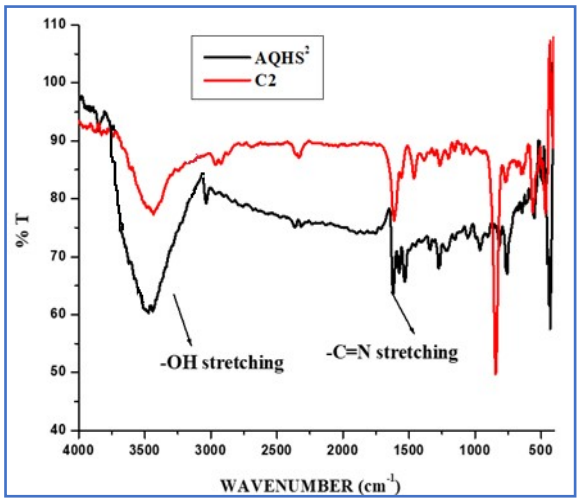


**Fig. S2.** IR spectra of ligand **AQHS[2]** and complex**C2**

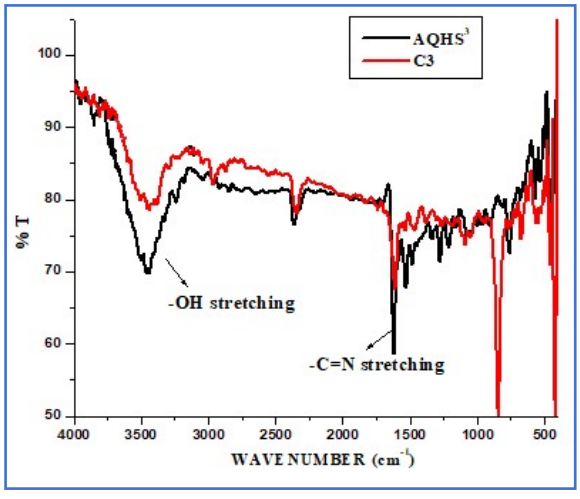


**Fig. S3.** IR spectra of ligand **AQHS[3]** and complex**C3**

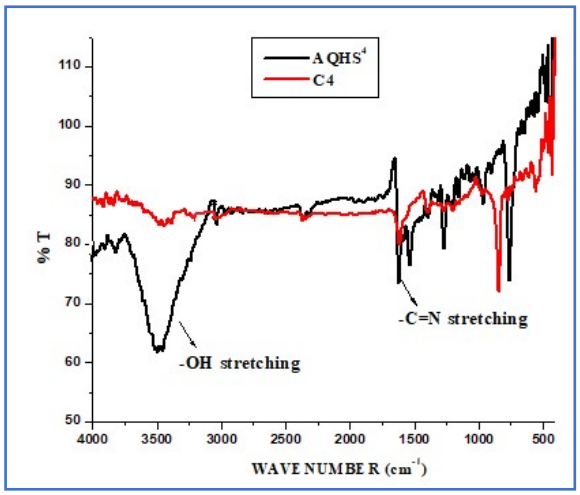


**Fig. S4.** IR spectra of ligand **AQHS$^4$** and complex**C4**

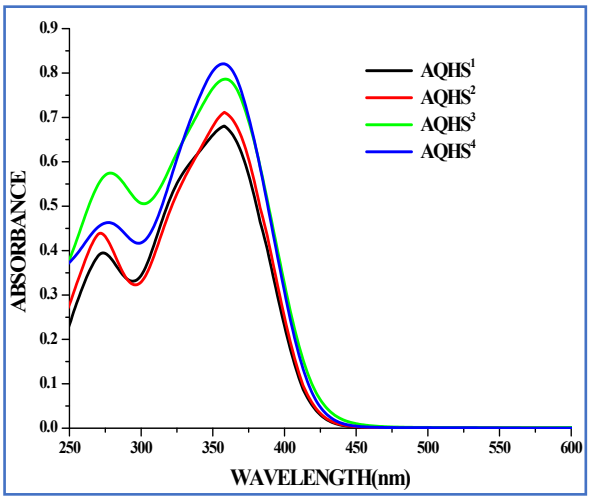


**Fig. S5.** Electronic spectra of the ligands (**AQHS$^{1-4}$**) recorded in dimethylsulphoxide.

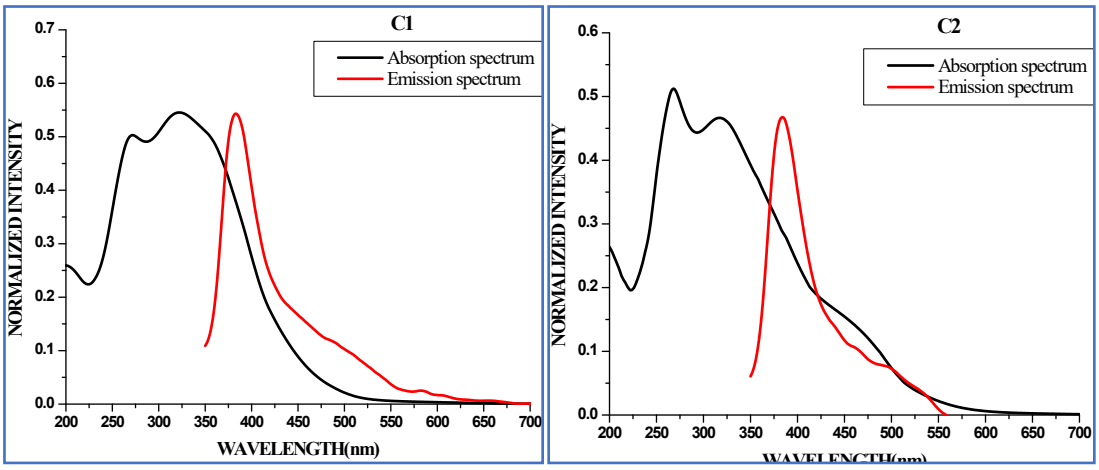

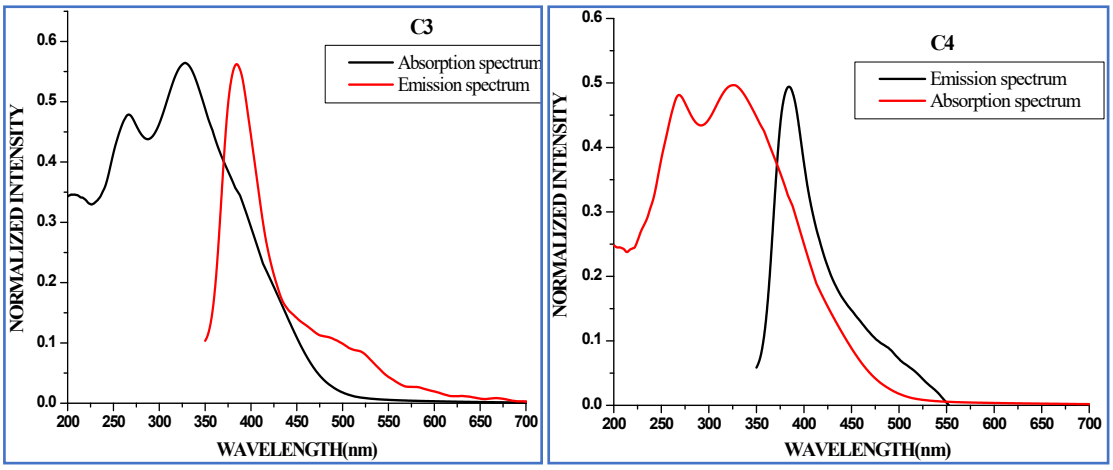


**Fig. S6.** Electronic and emission spectra of the complexes **C1-C4** recorded in dimethylsulphoxide, $\lambda_{ex}$= 330 nm.

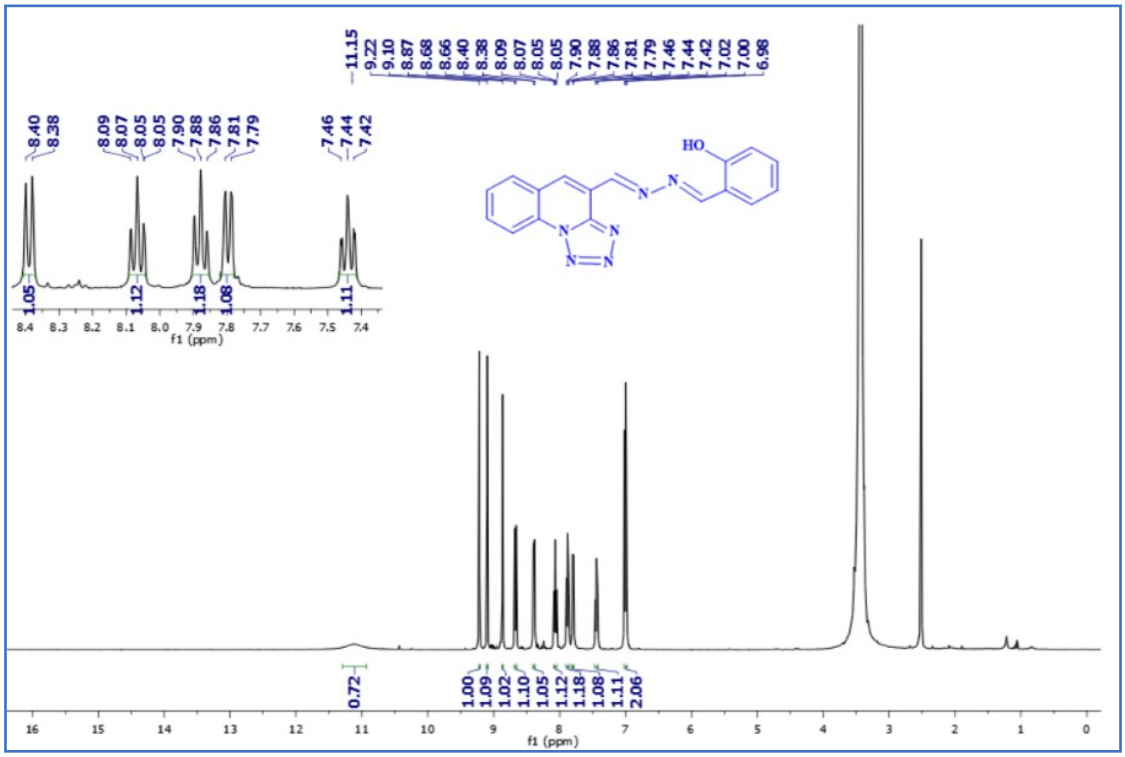


**Fig. S7.** $^{1}$H-NMR spectra of ligand **AQHS**[1]

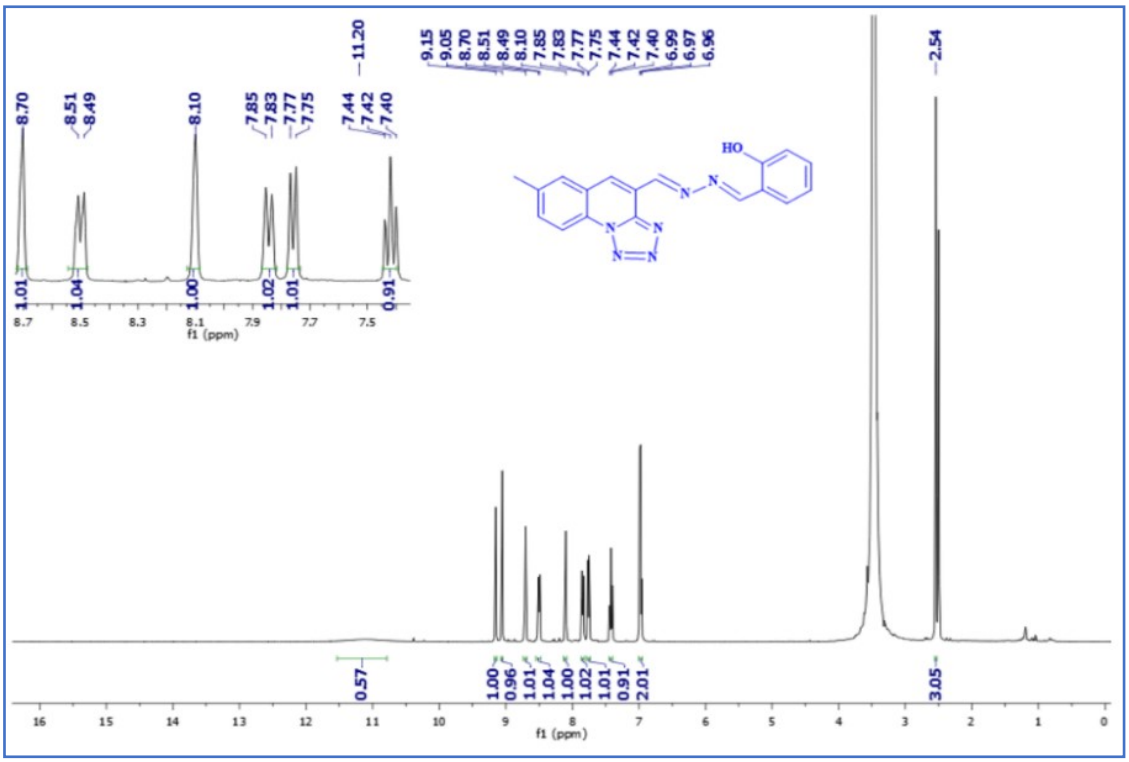


**Fig. S8.** [1]H-NMR spectra of ligand **AQHS[2]**

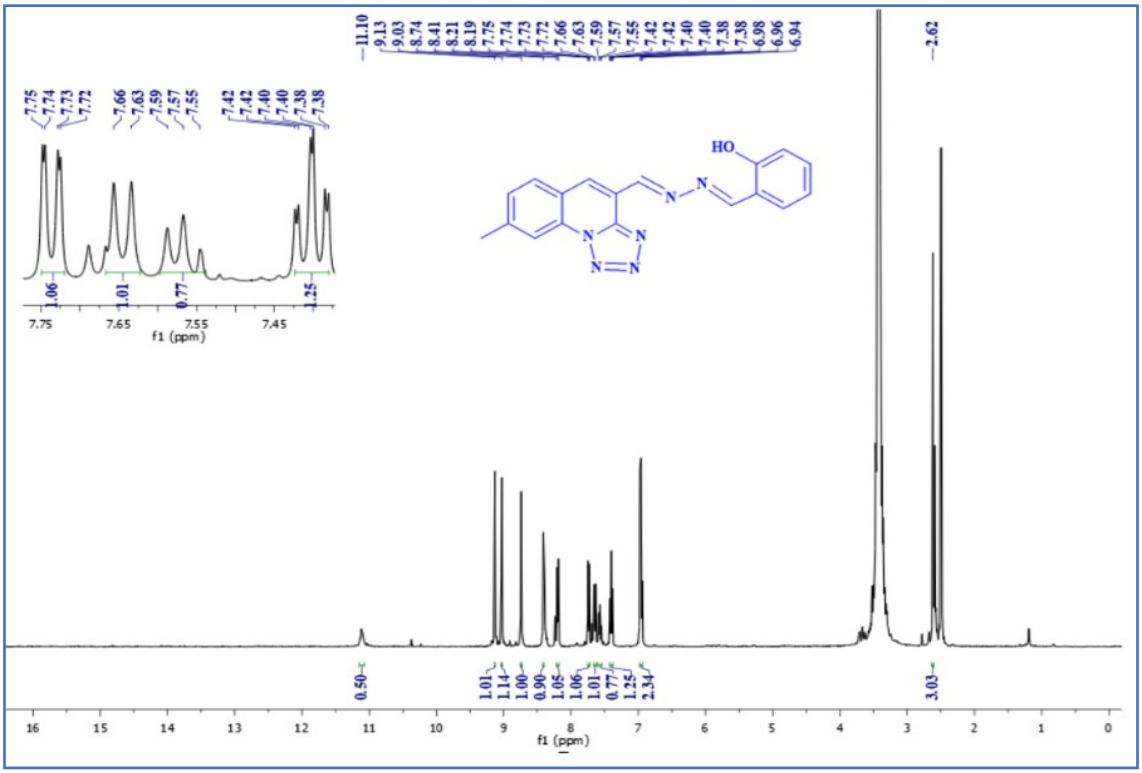


**Fig. S9.** [1]H-NMR spectra of ligand **AQHS[3]**

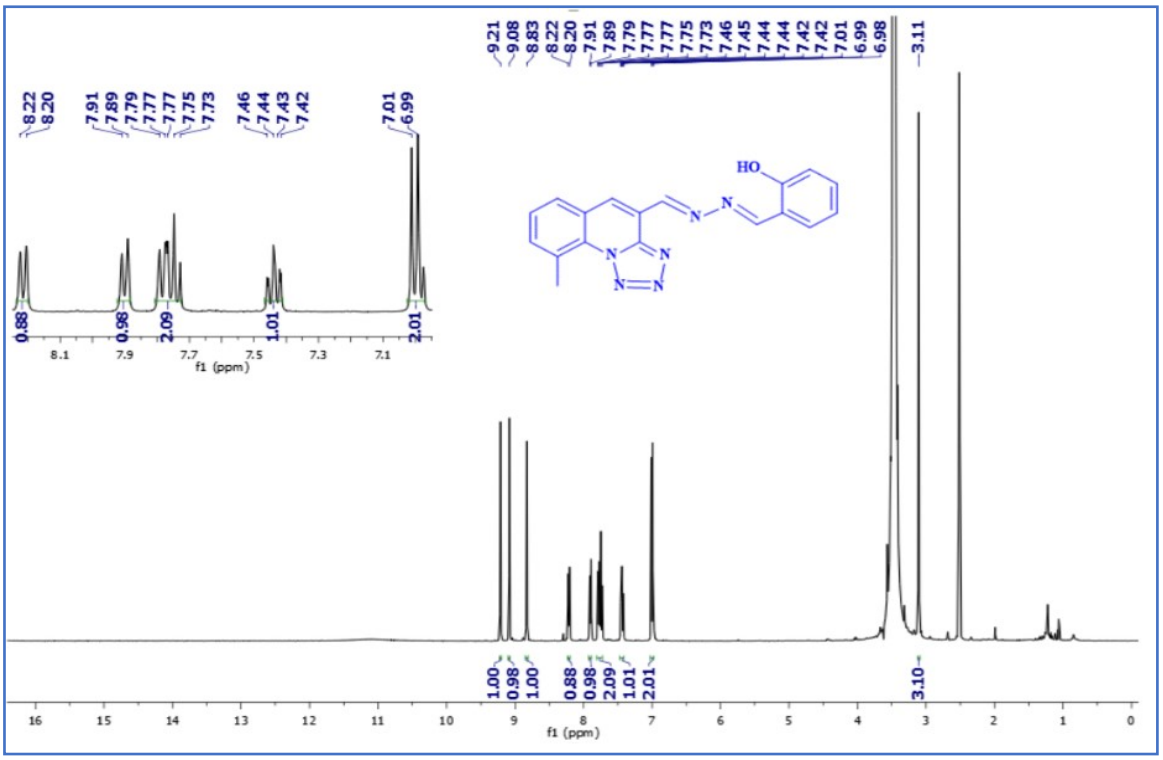


**Fig. S10.** [1]H-NMR spectra of ligand **AQHS**[4]

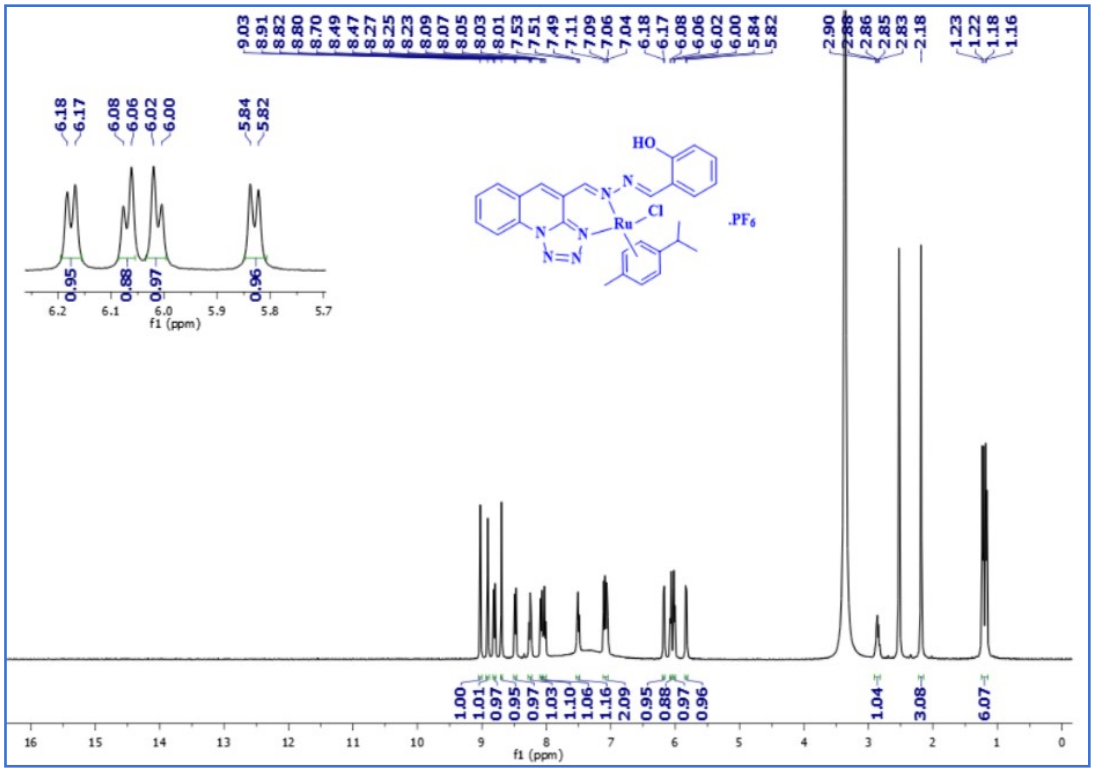


**Fig. S11.** [1]H-NMR spectra of complex **C1**

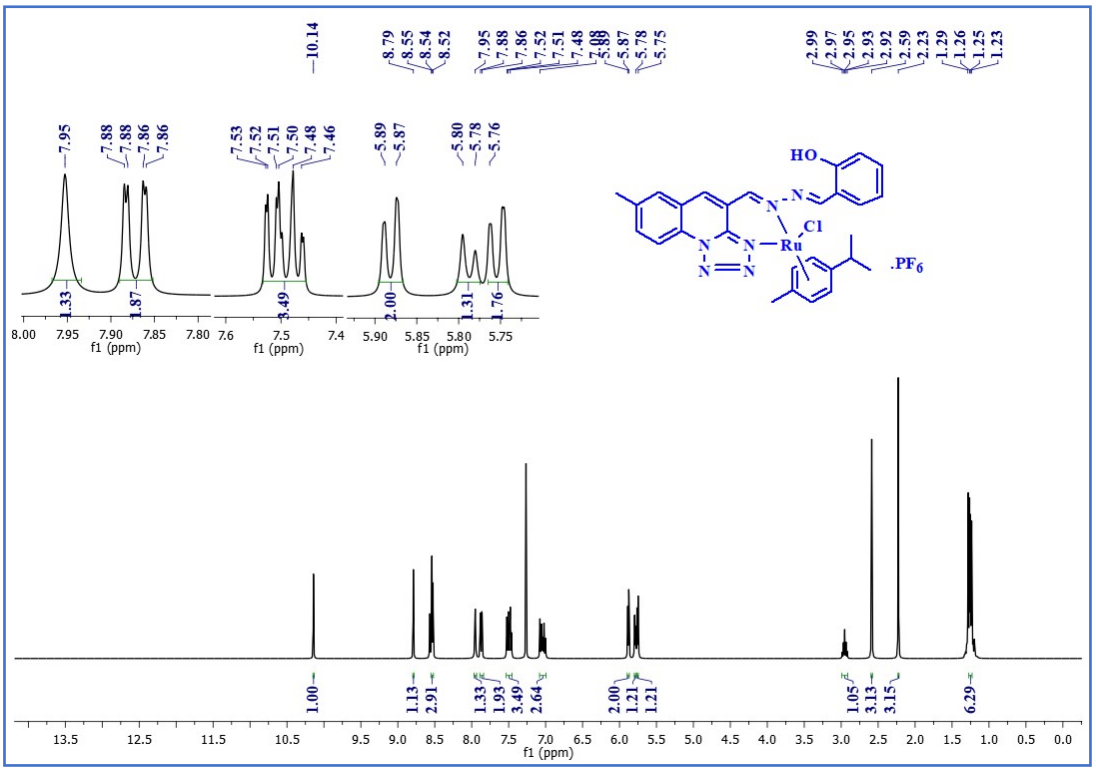


**Fig. S12.** [1]H-NMR spectra of complex **C2**

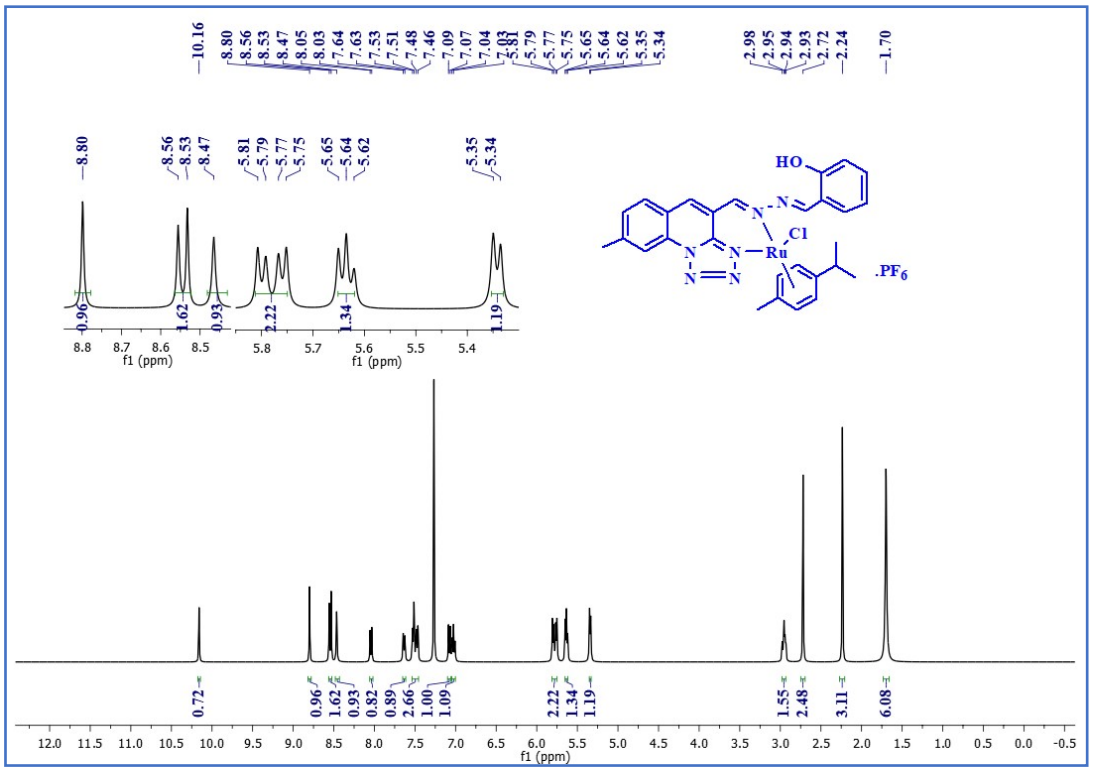


**Fig. S13.** [1]H-NMR spectra of complex **C3**

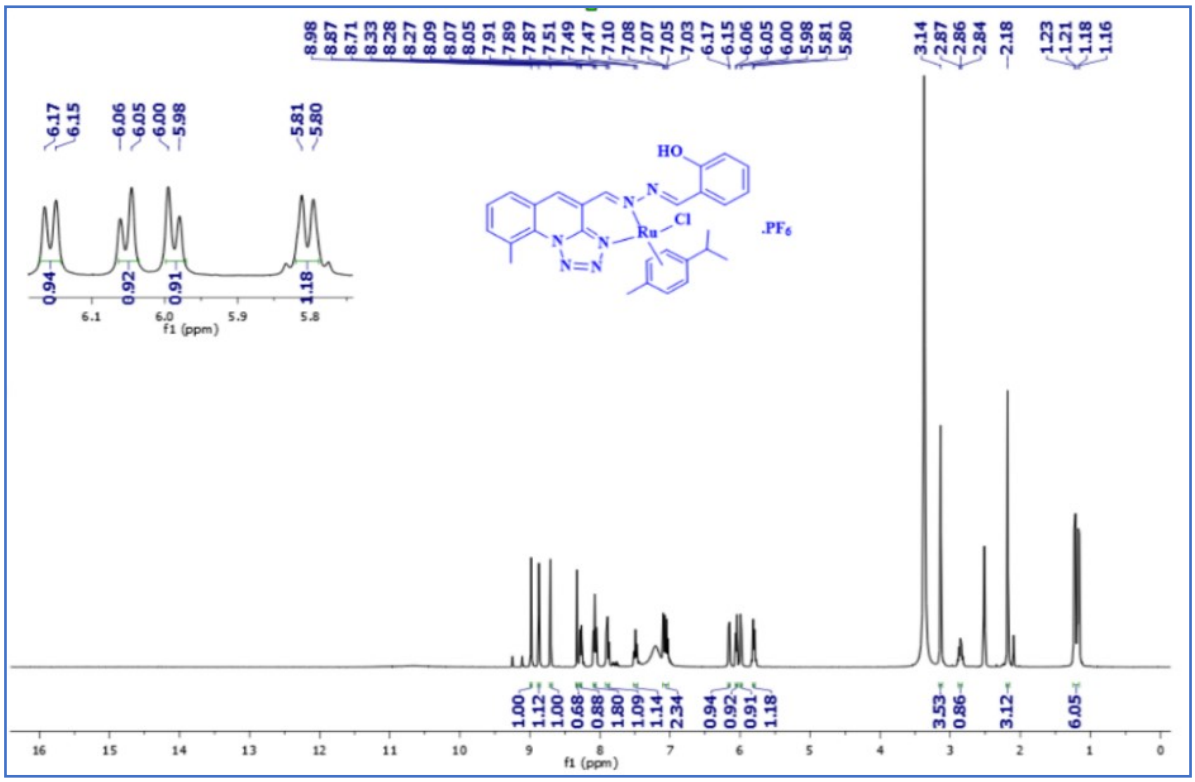


**Fig. S14.** $^{1}$H-NMR spectra of complex **C4**

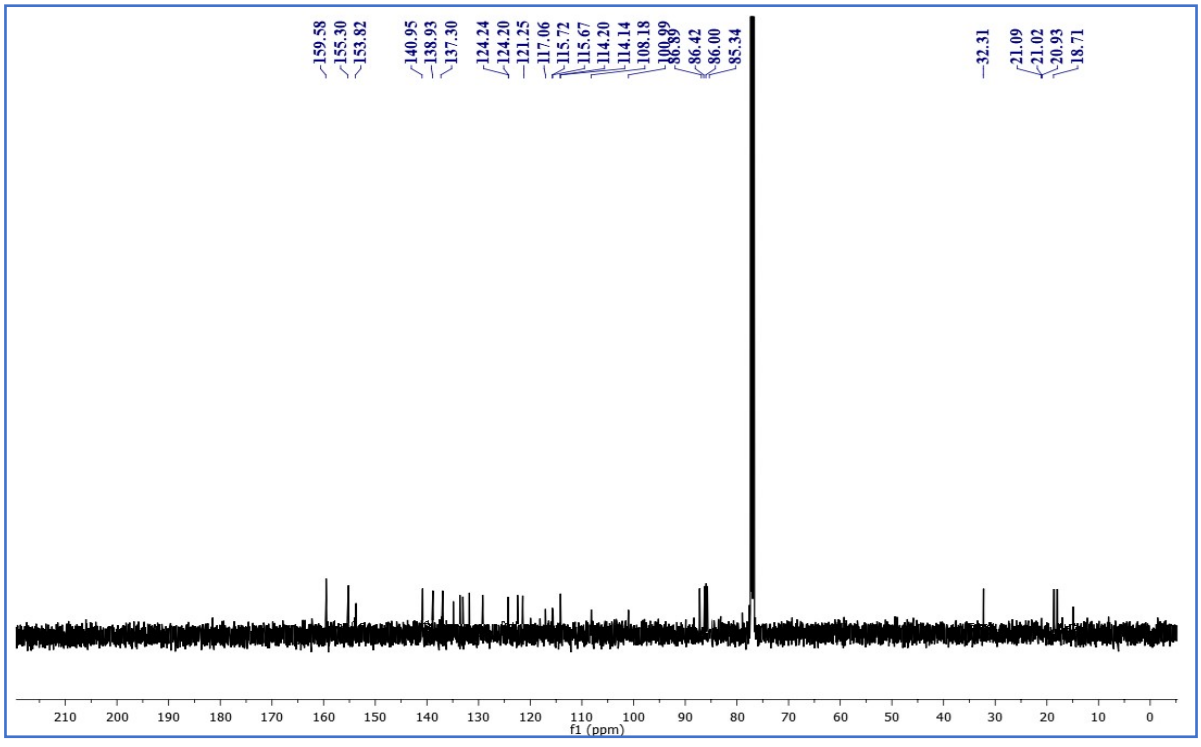


**Fig. S15.** $^{13}$C-NMR spectra of complex **C1**

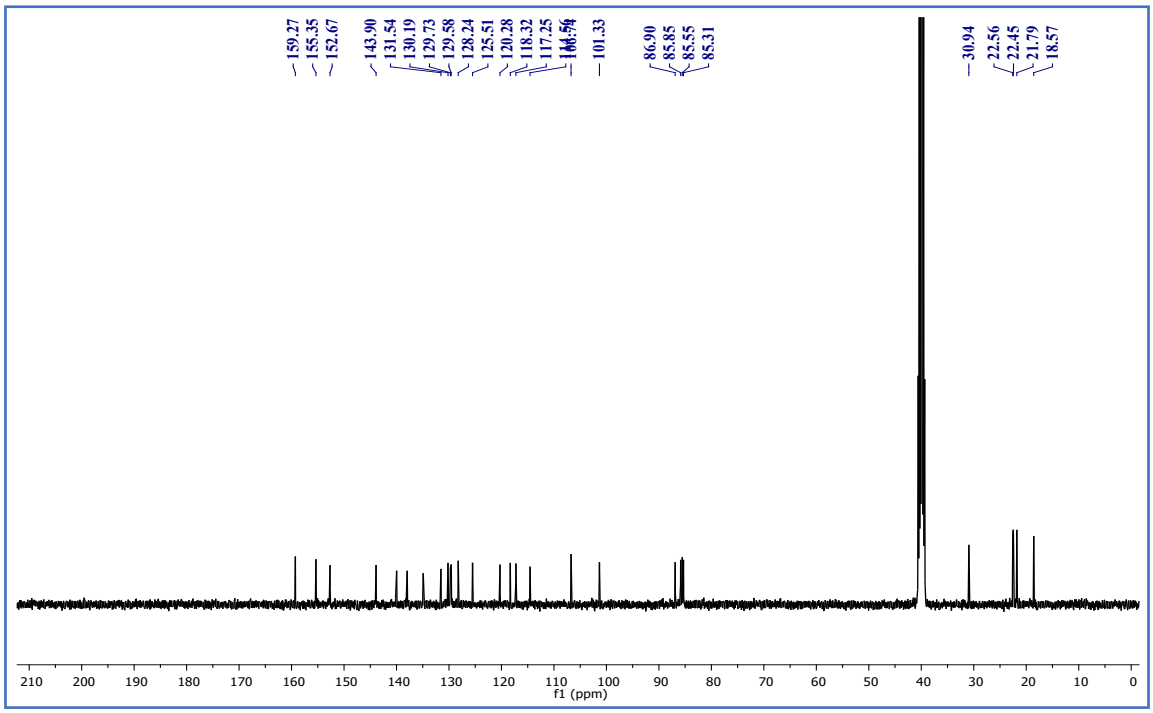


**Fig. S16.** $^{13}$C-NMR spectra of complex **C2**

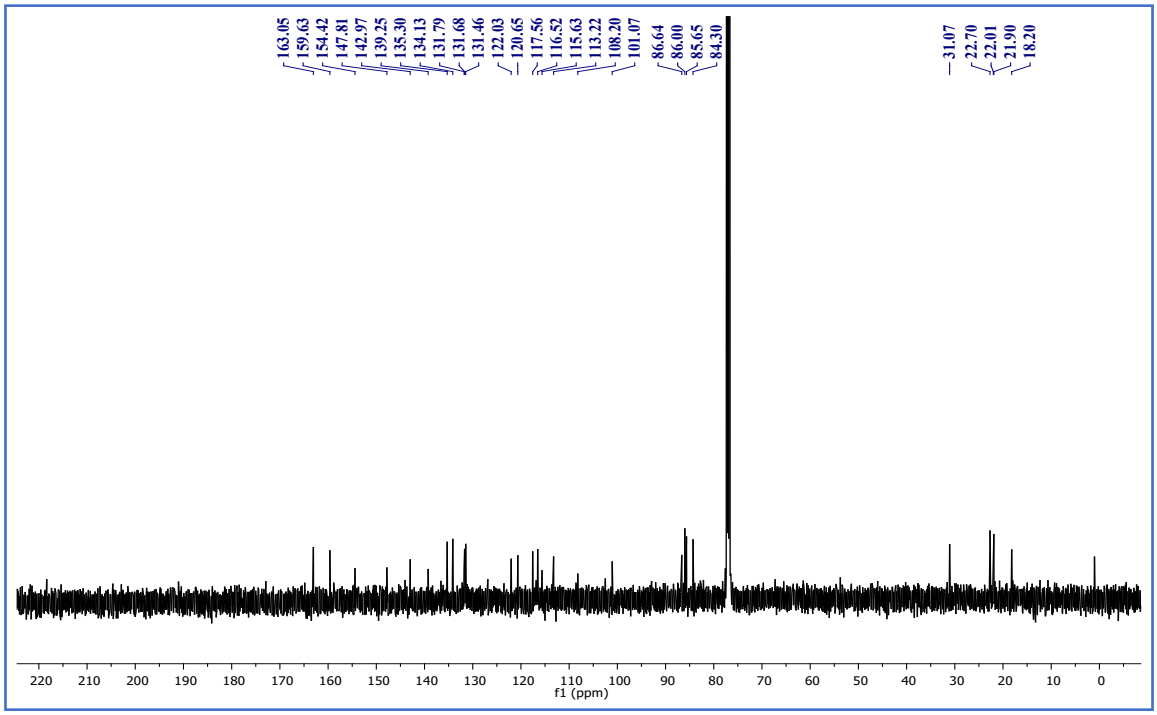


**Fig. S17.** $^{13}$C-NMR spectra of complex **C3**

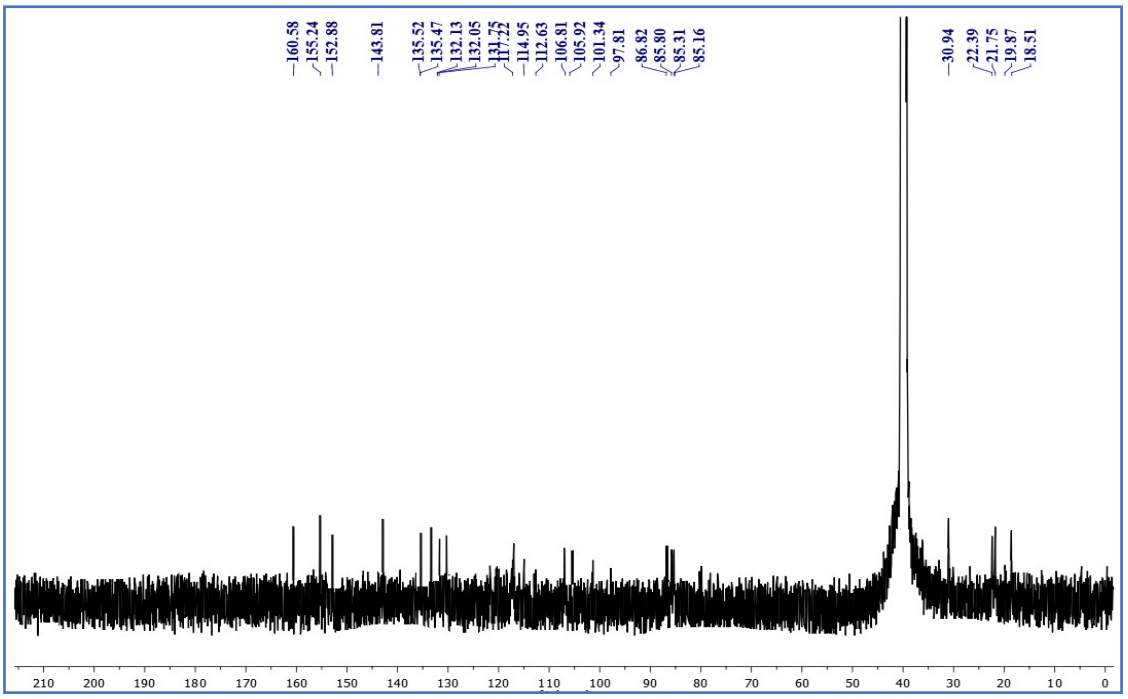


**Fig. S18.** $^{13}$C-NMR spectra of complex **C4**

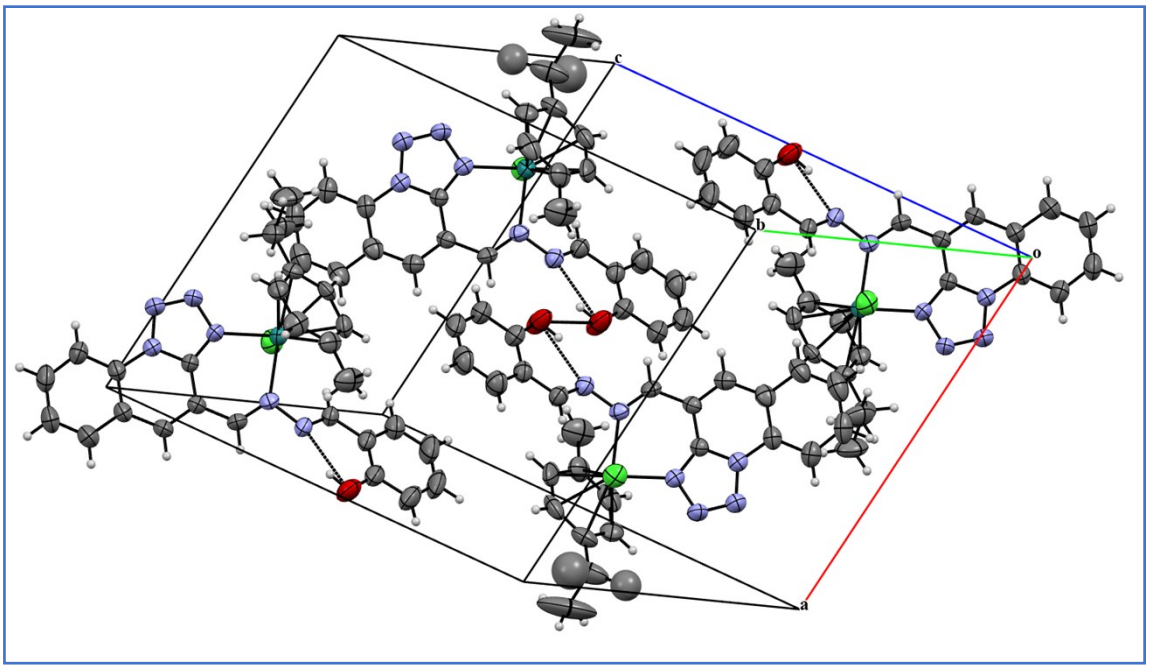


**Fig. S19.** Molecular packing diagram of the complex **C1**

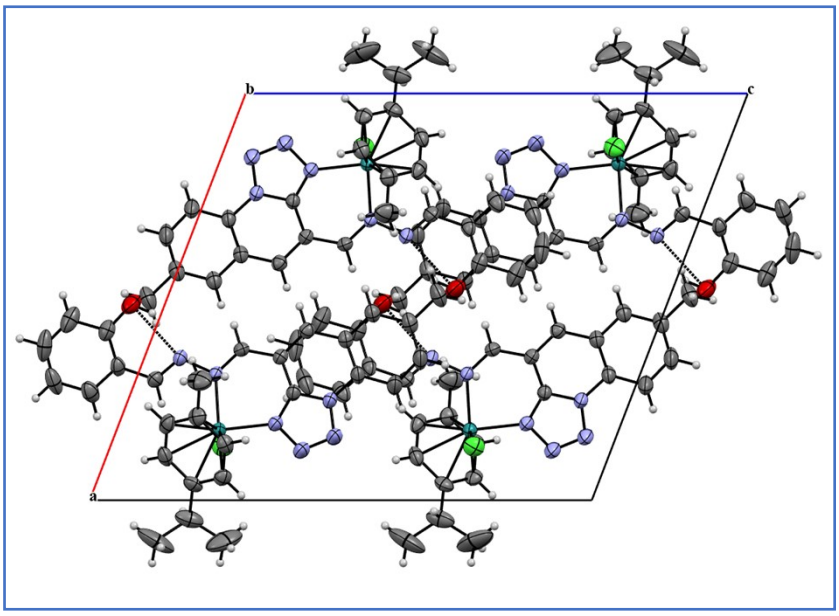


**Fig. S20.** Molecular packing diagram of the complex **C2**

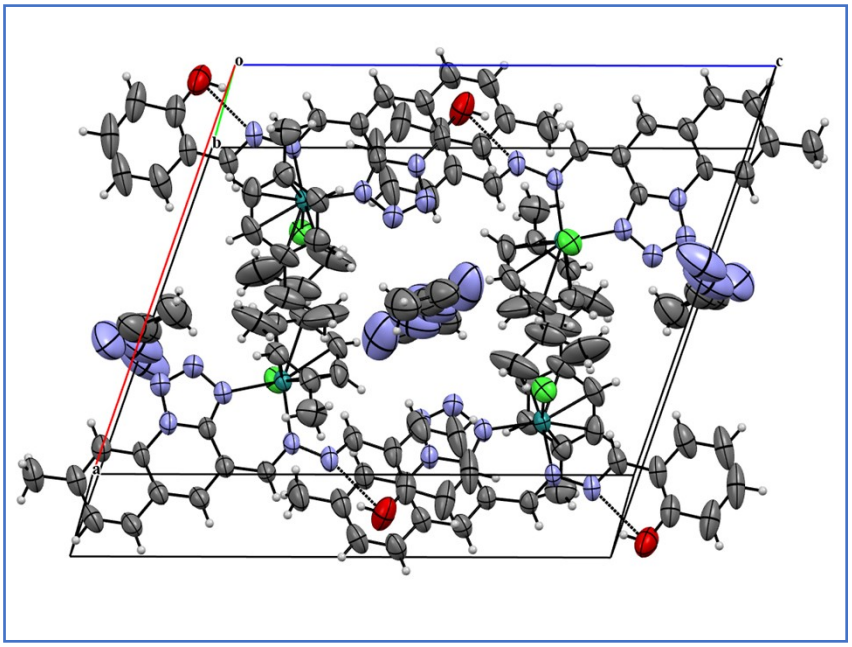


**Fig. S21.** Molecular packing diagram of the complex **C3**

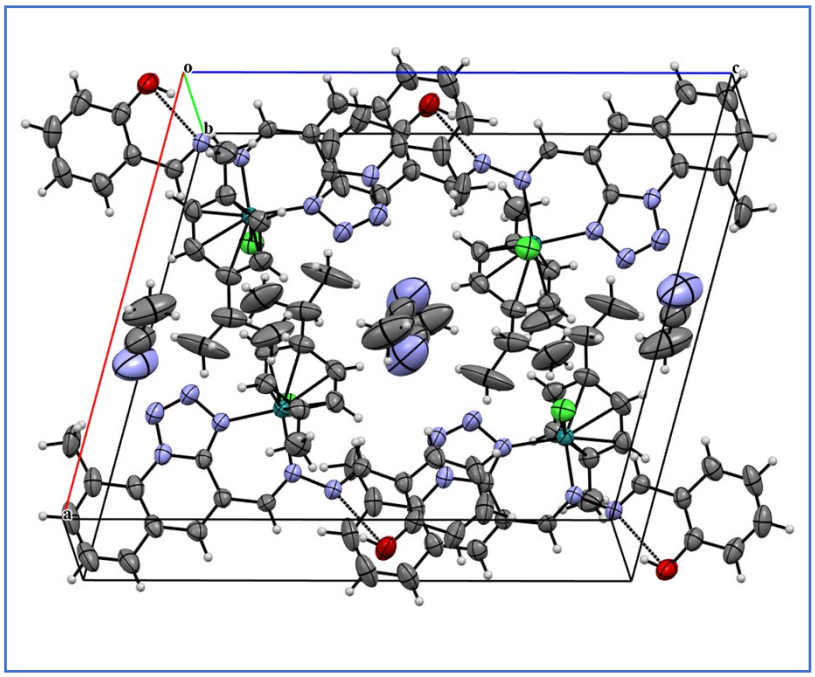


**Fig. S22.** Molecular packing diagram of the complex **C4**

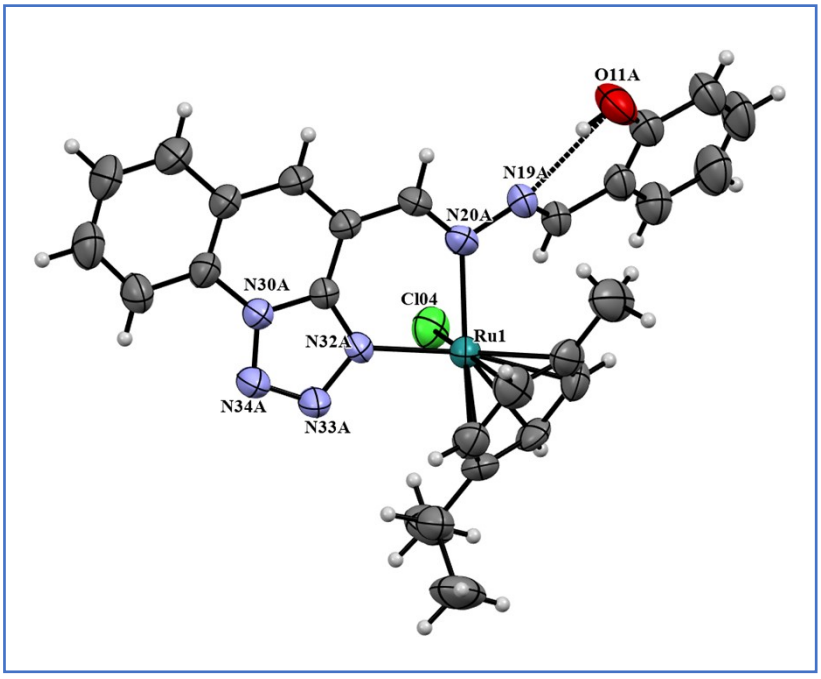


**Fig. S23.** ORTEP diagram of the complex **C1** with hydrogen bonding

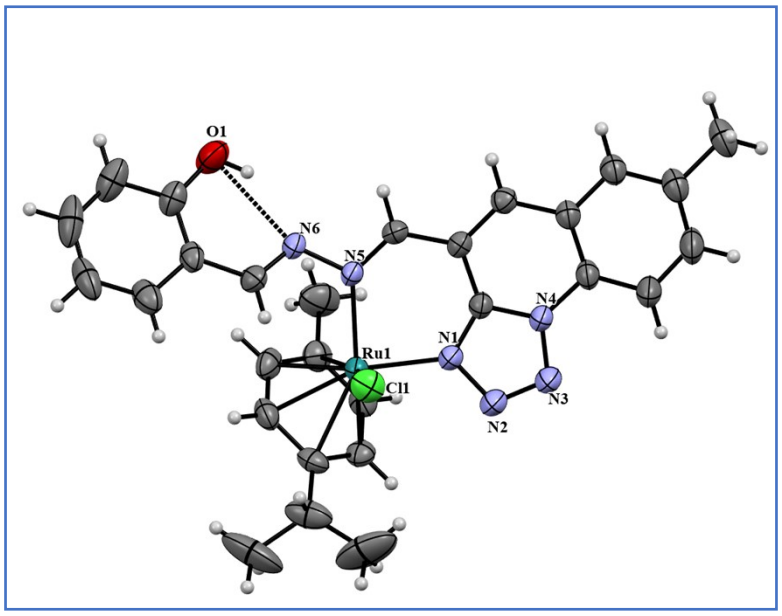


**Fig. S24.** ORTEP diagram of the complex **C2** with hydrogen bonding

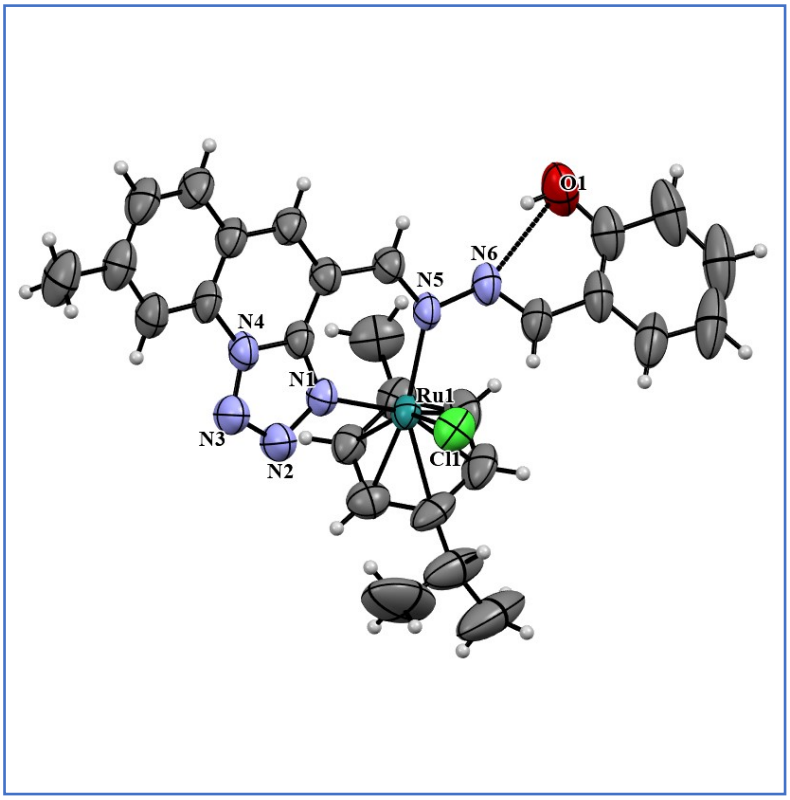


**Fig. S25.** ORTEP diagram of the complex **C3** with hydrogen bonding

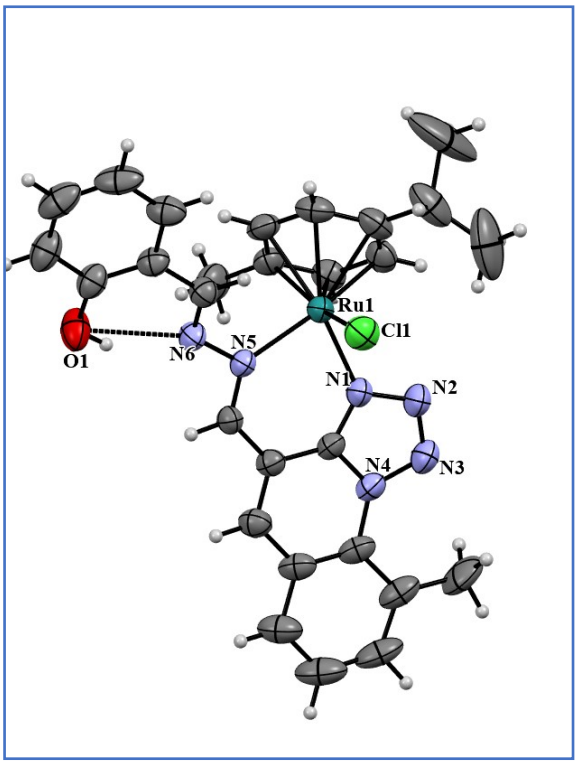


**Fig. S26.** ORTEP diagram of the complex **C4** with hydrogen bonding

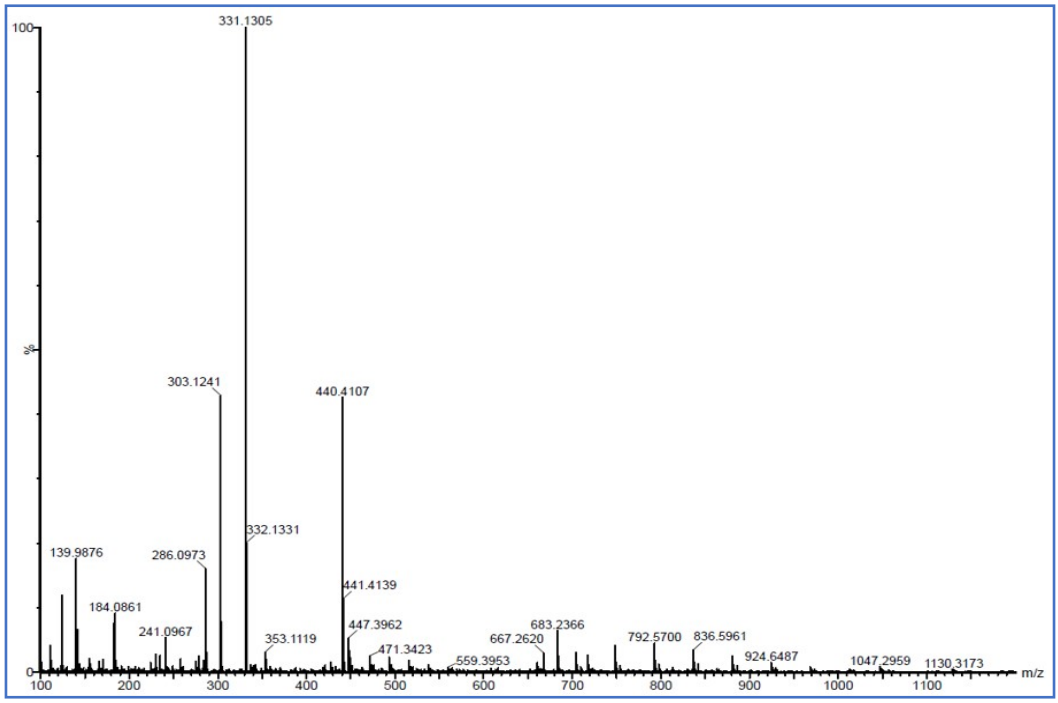


**Fig. S27.** Mass spectrum of the ligand **AQHS**[4]

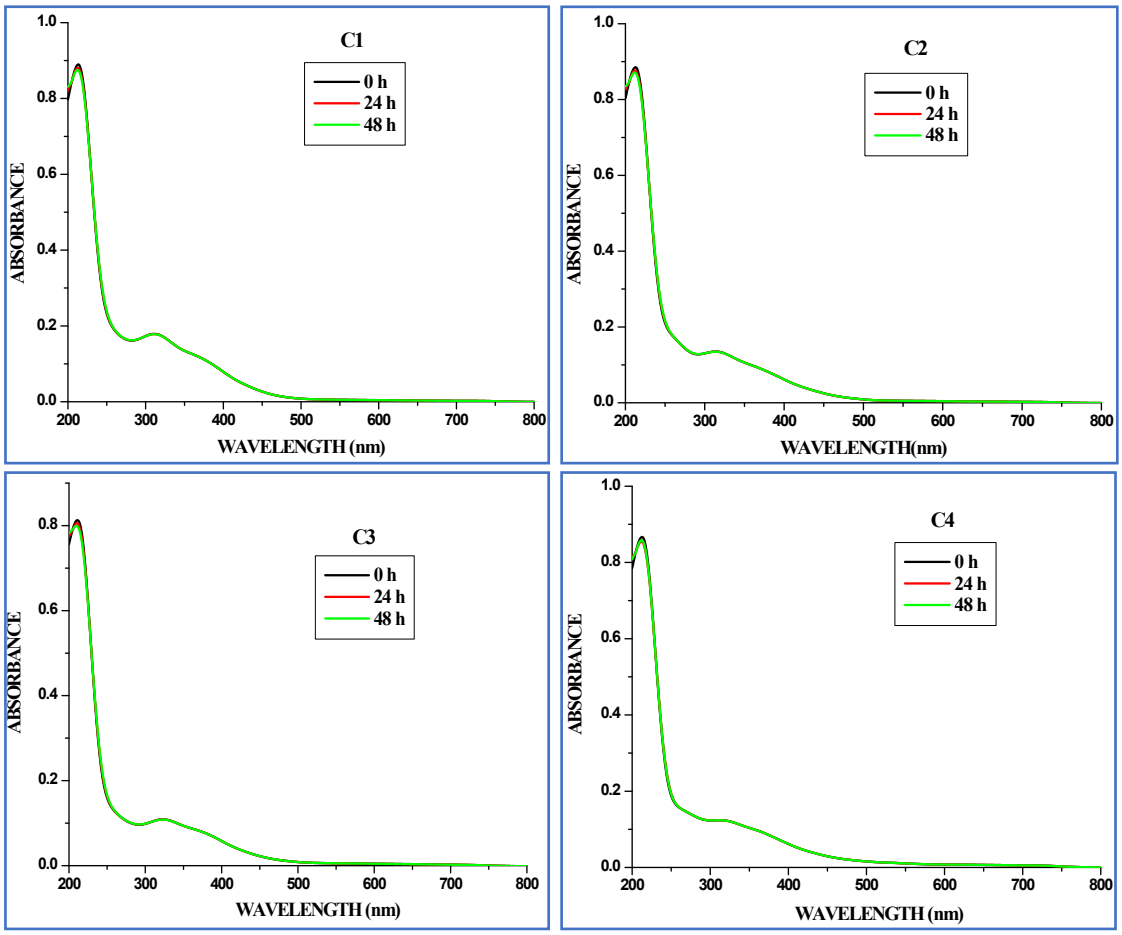


**Figure S28a.** Absorption spectra of the complexes (**C1 - C4**) [10 µM] at 0 - 48 h time intervals at 20°C in Tris-HCl buffer (pH-7.2)

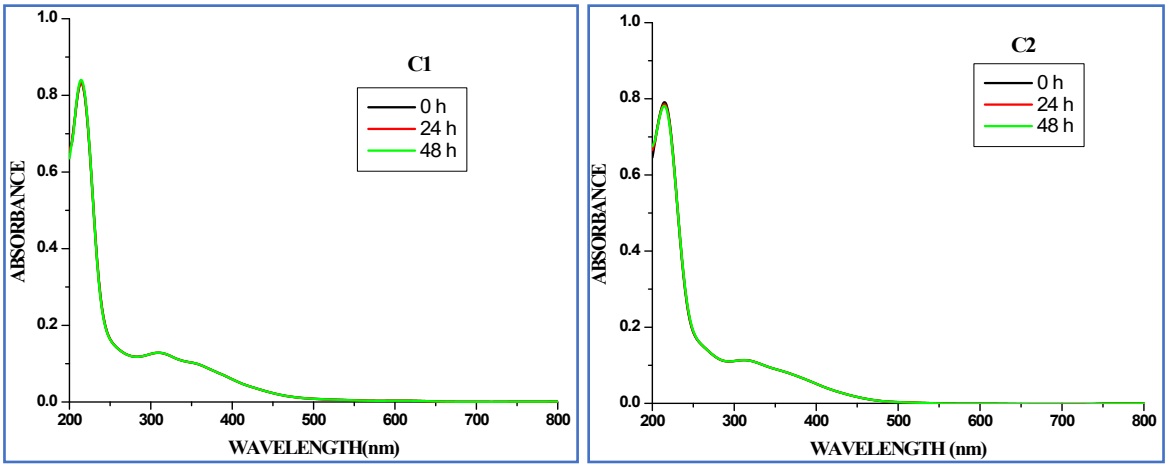

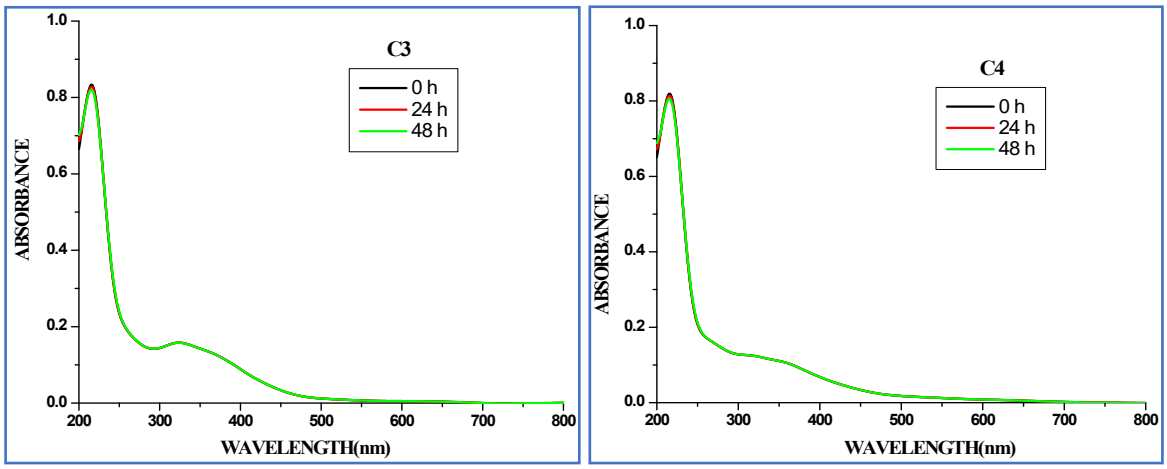


**Figure S28b.** Absorption spectra of the complexes (**C1 - C4**) [10 µM] at 0 - 48 h time intervals at 20°C in phosphate buffer (pH-7.4)

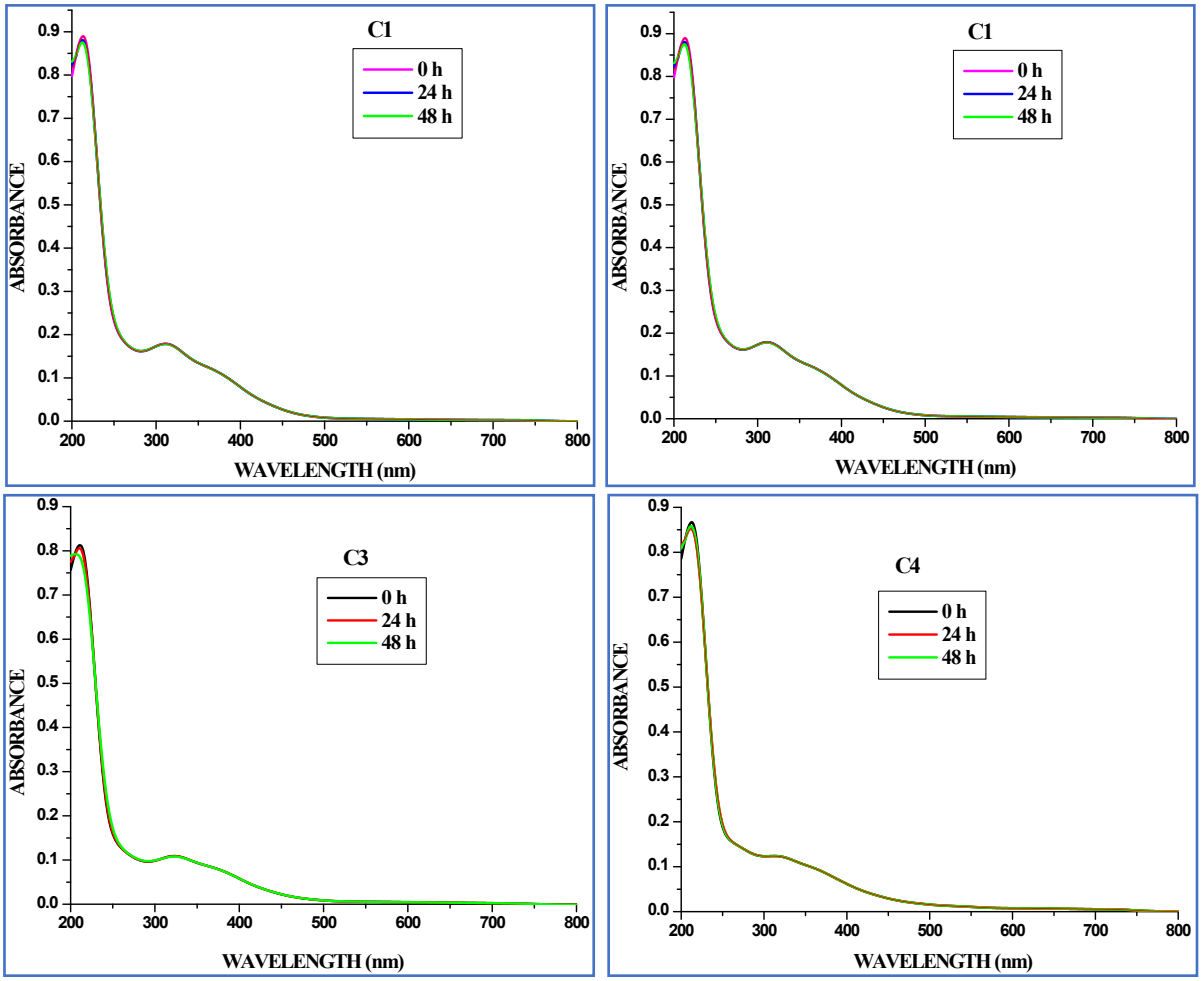


**Fig. S29a.** Absorption spectra of the complexes (**C1 - C4**) [10 µM] at 0 - 48 h time intervals at room temperature in Tris-HCl buffer (pH-7.2)

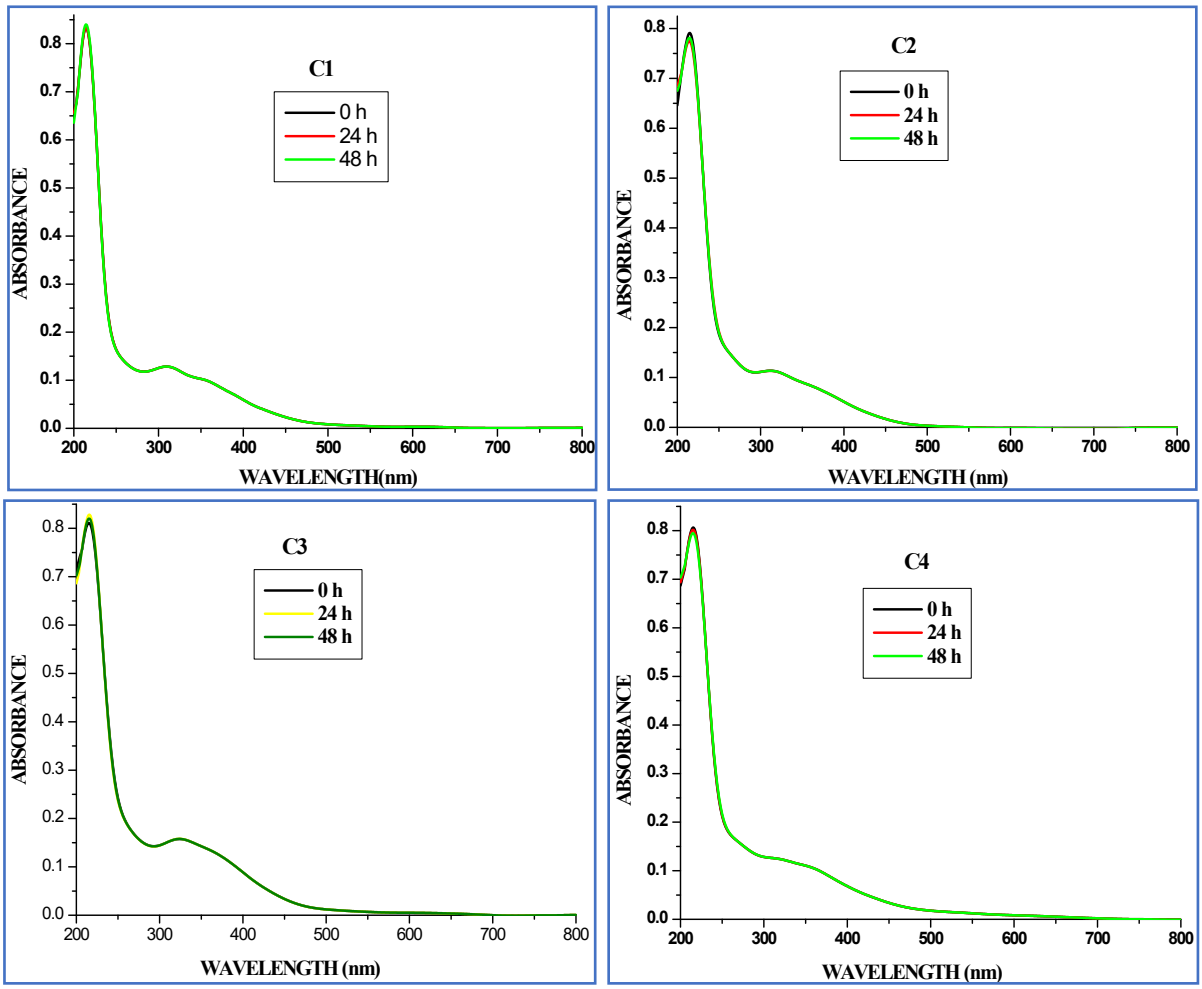


**Fig. S29b.** Absorption spectra of the complexes (**C1 - C4**) [10 µM] at 0 - 48 h time intervals at room temperature in phosphate buffer (pH-7.4)

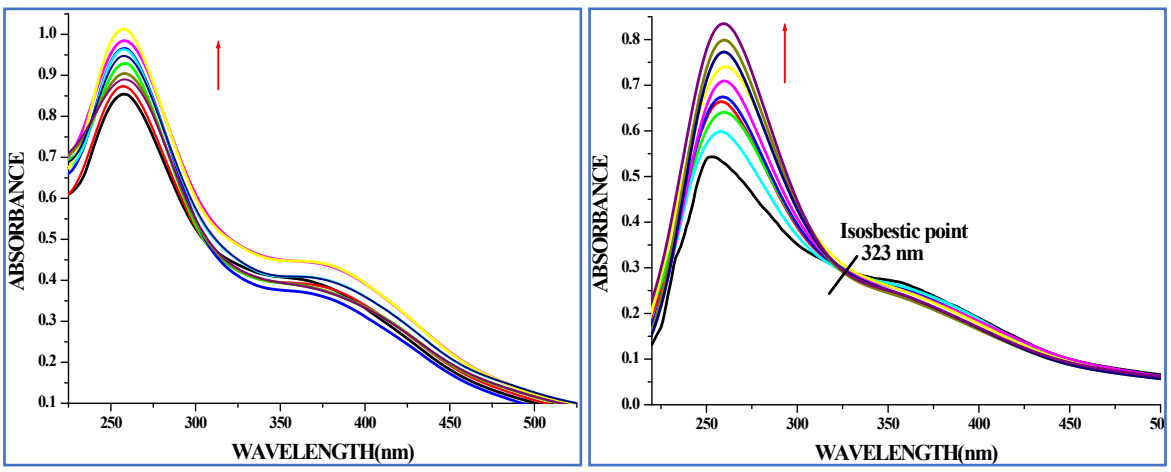

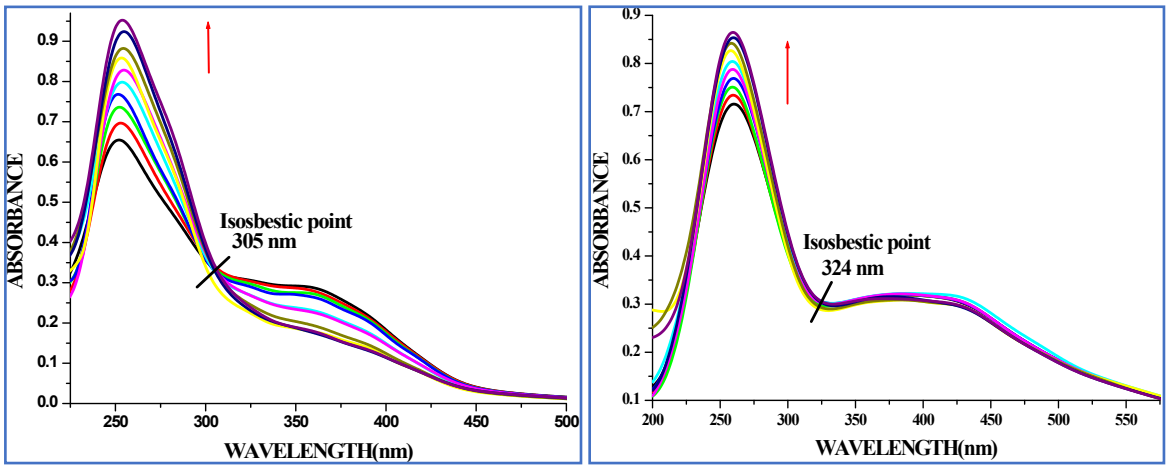


**Fig. S30.** Absorption spectra of ligands (**AQHS**$^{1\text{-}4}$) (10 µM) with increasing concentrations of DNA (0-10 µM) (Tris-HCl buffer, NaCl, pH 7.2).

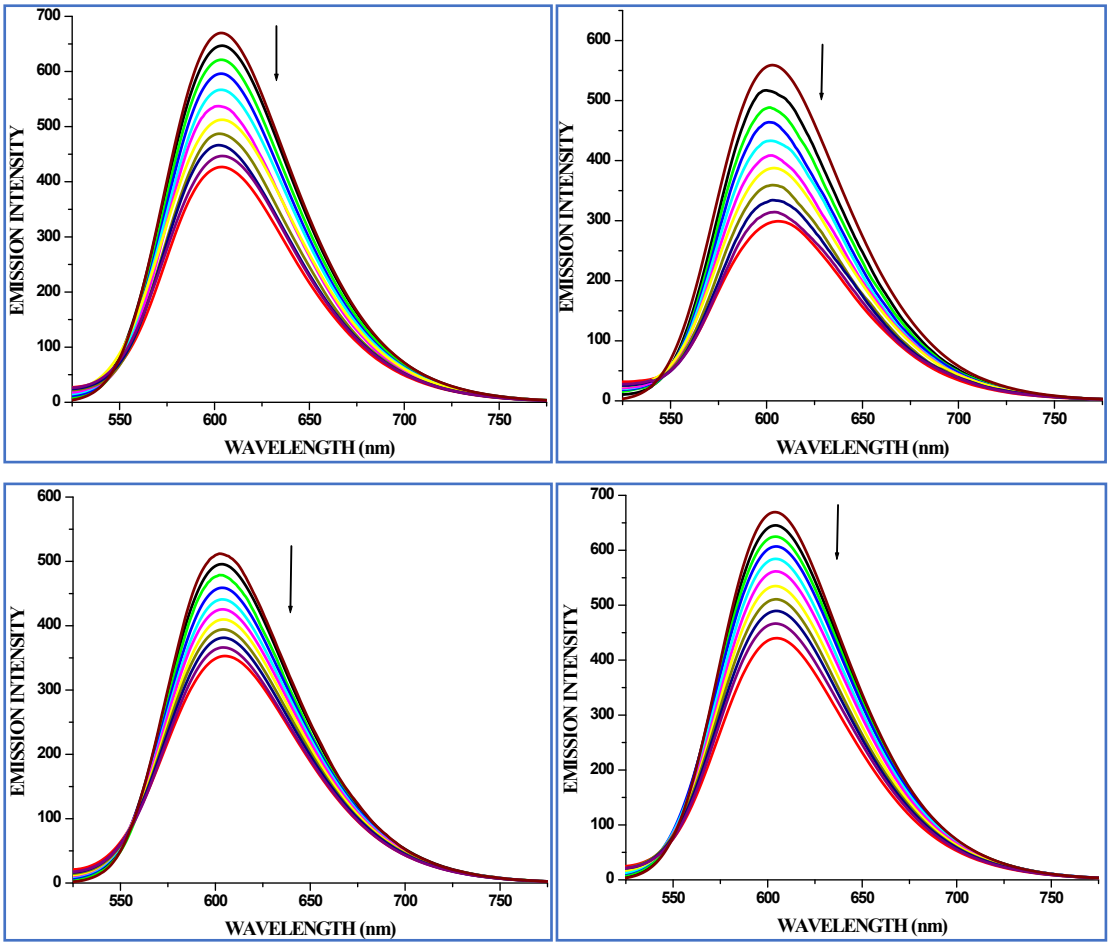


**Fig. S31.** Emission titration spectra of the CT-DNA (Tris-HCl buffer, pH-7.2) in presence of ligands. [DNA] = 10 µM, [EB] = 10 µM, [Ligands] = 10-100 µM. The arrows show the decrease in intensities upon an increasing in the concentration of the ligands.

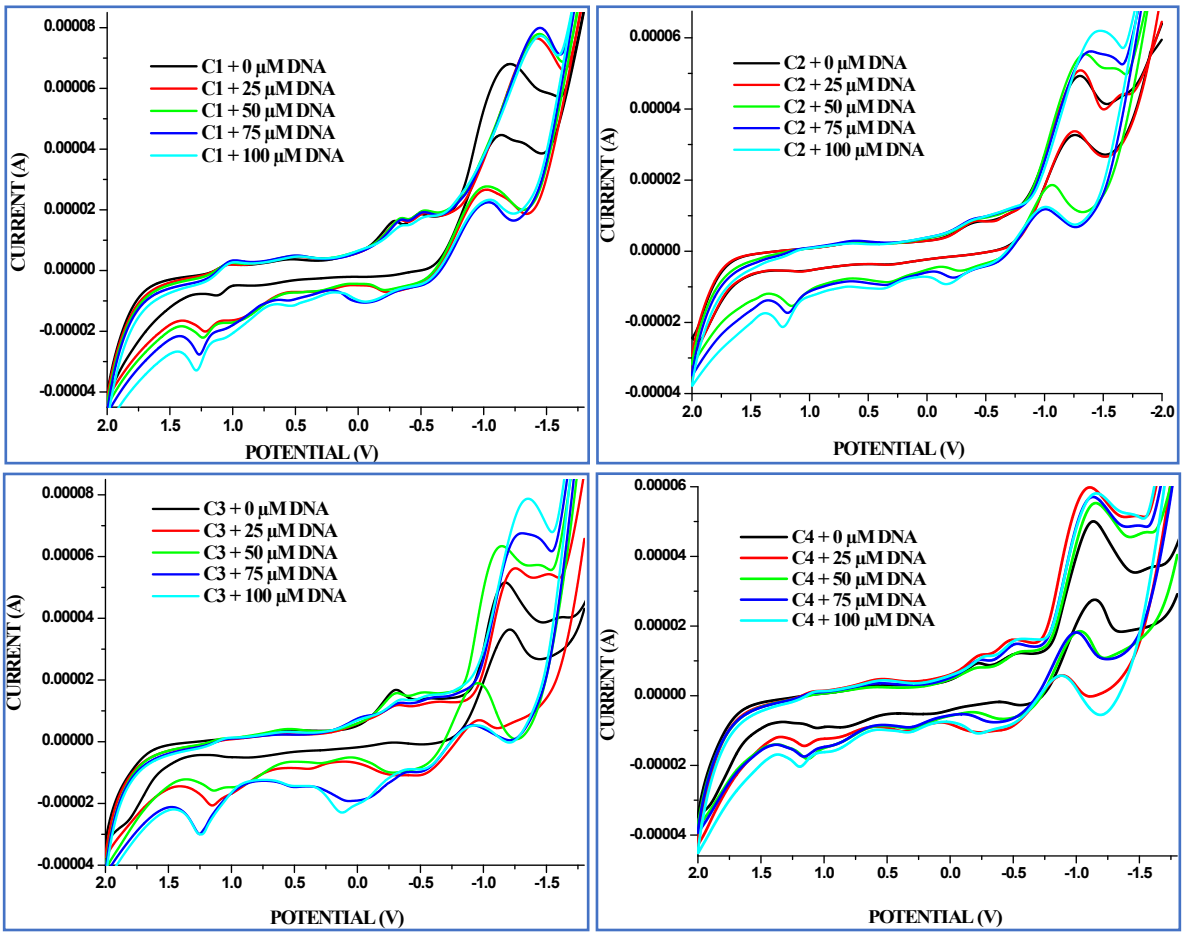


**Fig. S32.** Cyclic voltammograms of the complexes **C1-C4** in absence and presence of CT-DNA

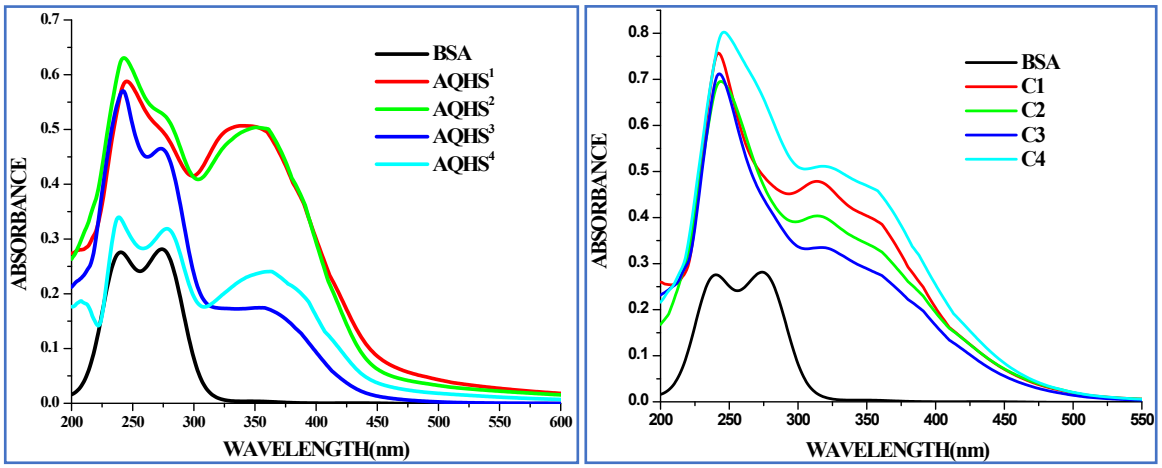


**Fig. S33.** Absorption spectra of free BSA and BSA with ligands (**AQHS$^{1-4}$**) and complexes (**C1 - C4**) at 10 µM concentration.

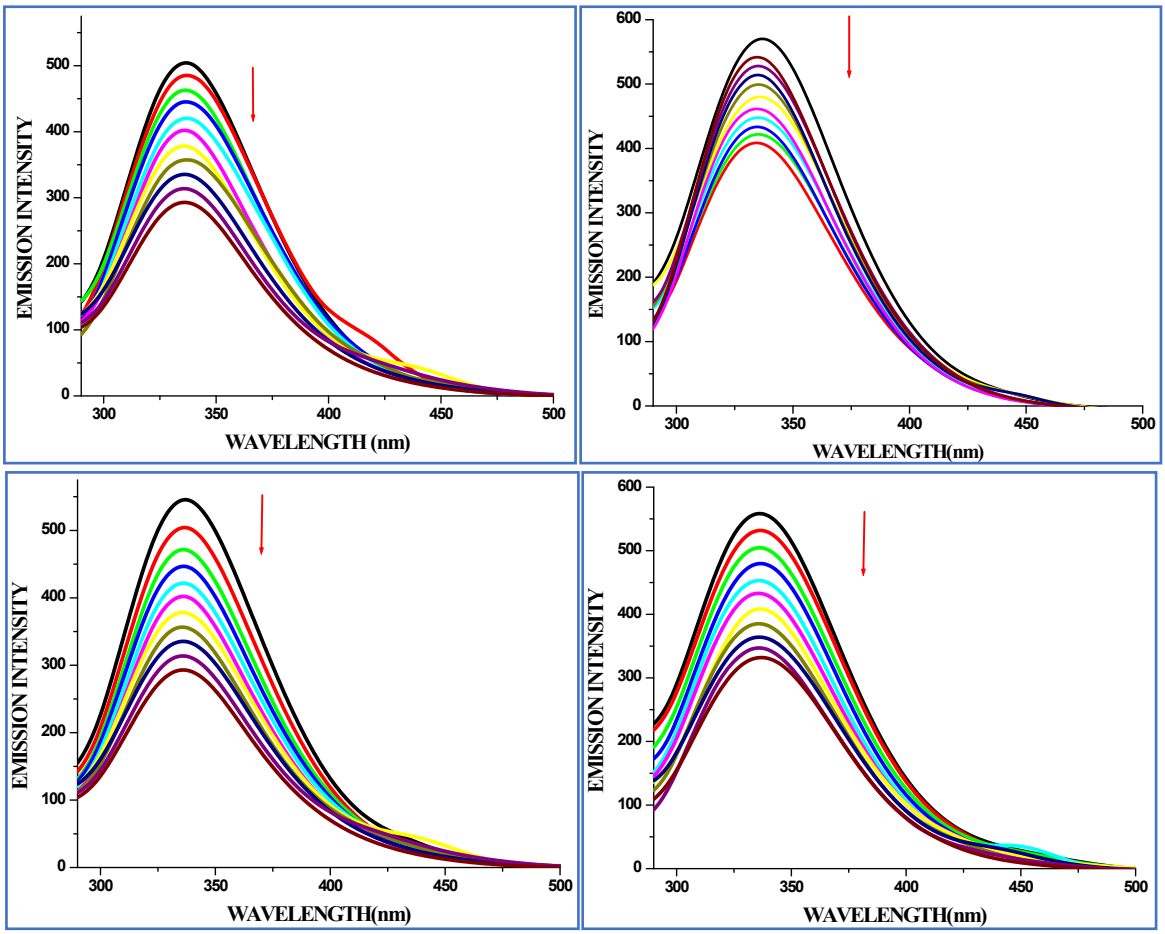


**Fig. S34.** The emission spectra of BSA (10 μM; $\lambda_{exc}$ = 280 nm; $\lambda_{emi}$ = 346 nm) in the presence of increasing amounts of ligands (**AQHS$^{1-4}$**) (10-100 μM).

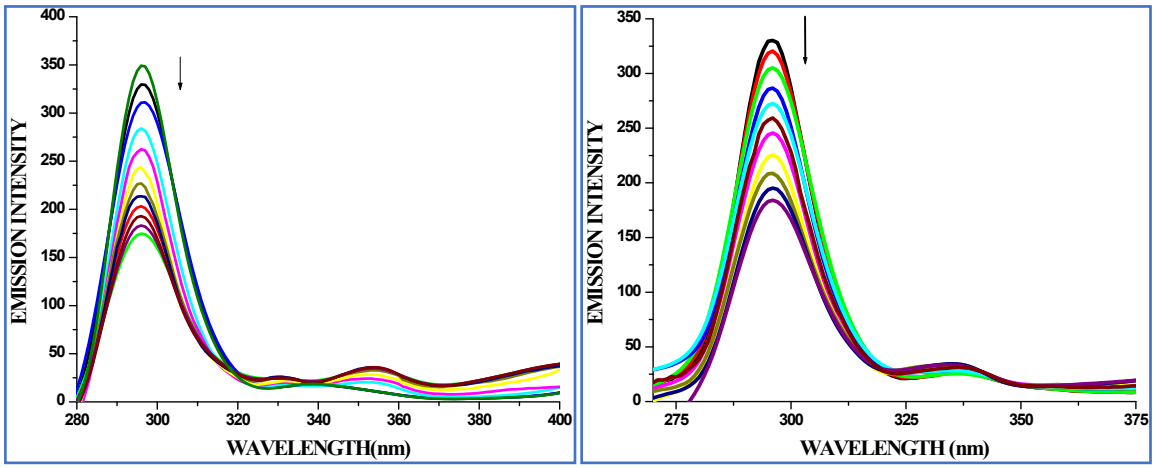

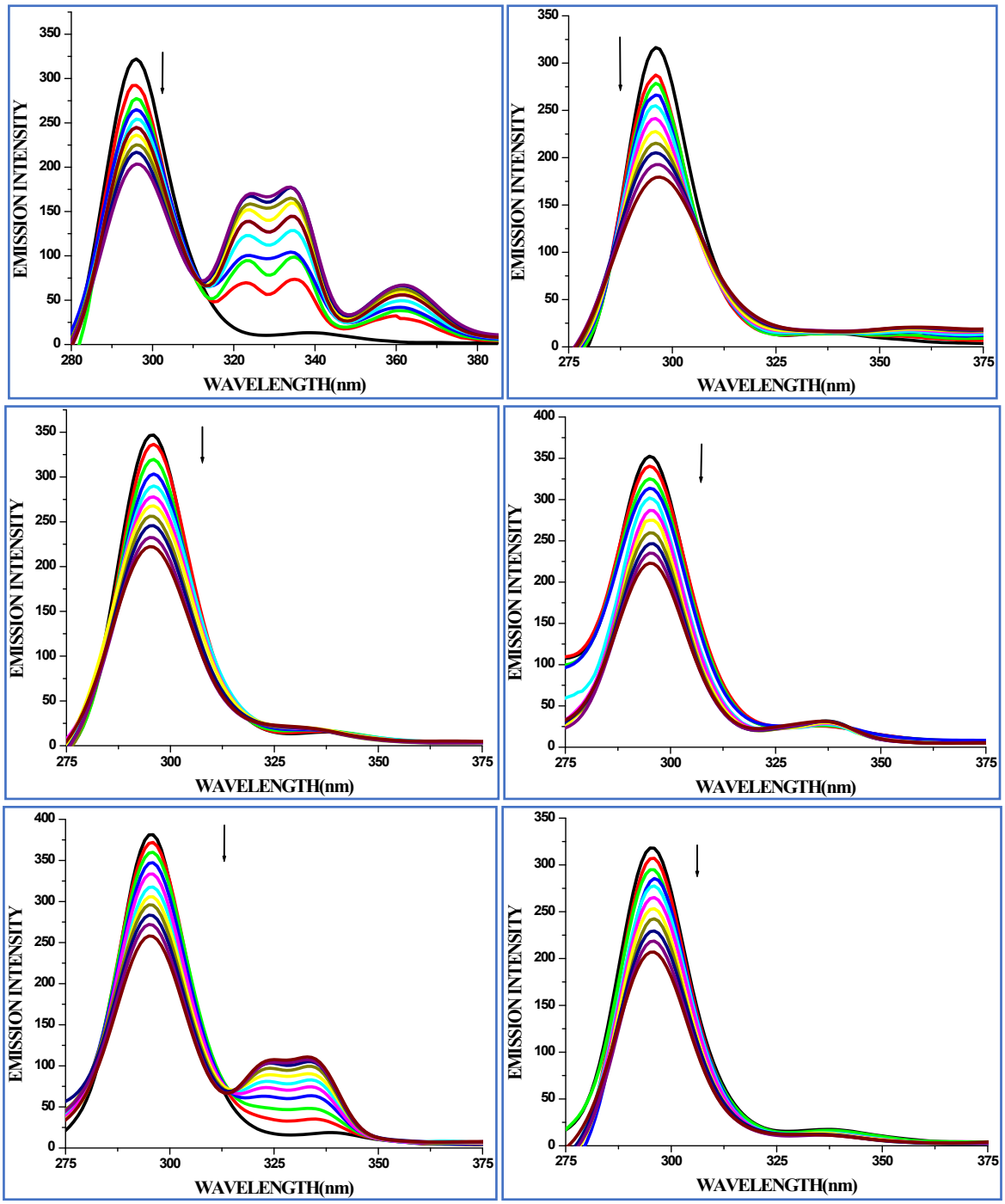


**Fig. S35.** Synchronous spectra of free BSA and BSA (10 μM) in the presence of increasing amounts of ligands (**AQHS$^{1-4}$**) and complexes (**C1-C4**) (10-100) μM concentration for wavelength difference of $\Delta\lambda$ = 15 nm.

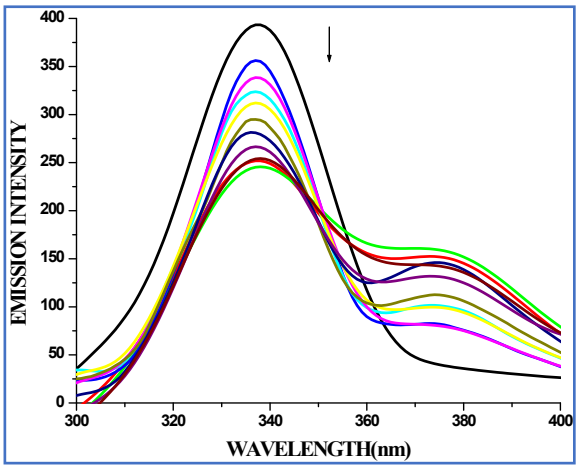
EMISSION INTENSITY
WAVELENGTH(nm)

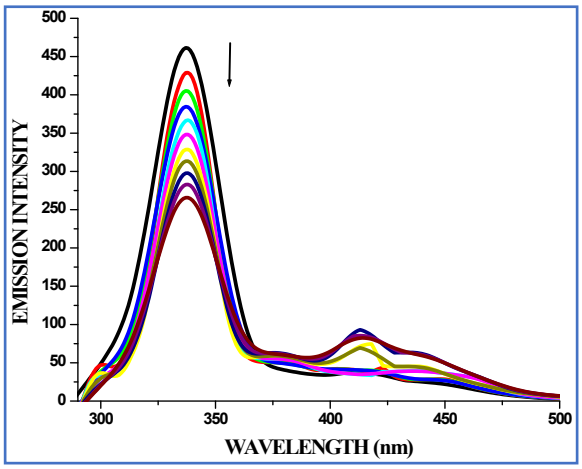
EMISSION INTENSITY
WAVELENGTH (nm)

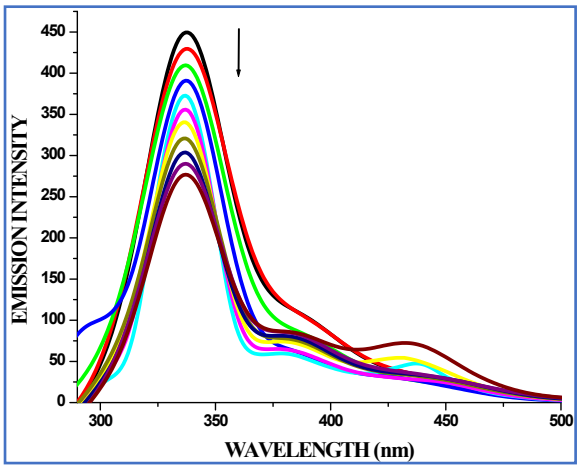
EMISSION INTENSITY
WAVELENGTH (nm)

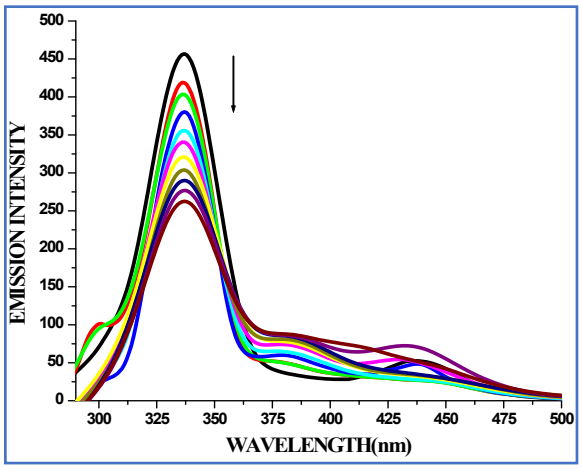
EMISSION INTENSITY
WAVELENGTH(nm)

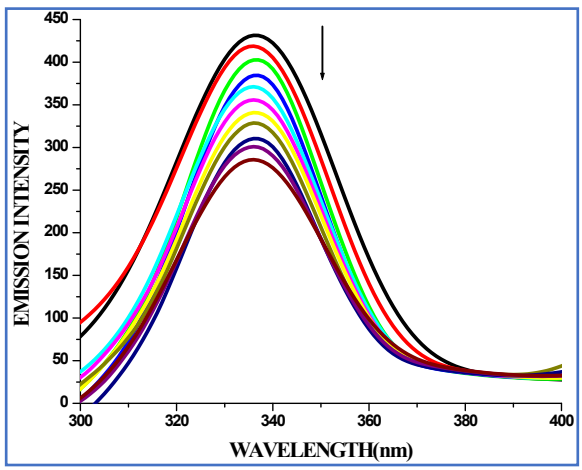
EMISSION INTENSITY
WAVELENGTH(nm)

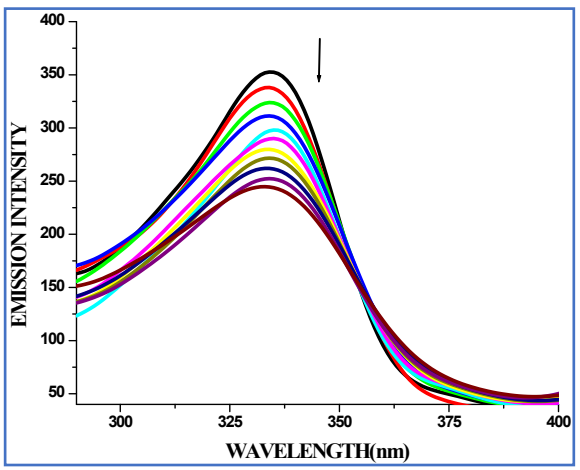
EMISSION INTENSITY
WAVELENGTH(nm)

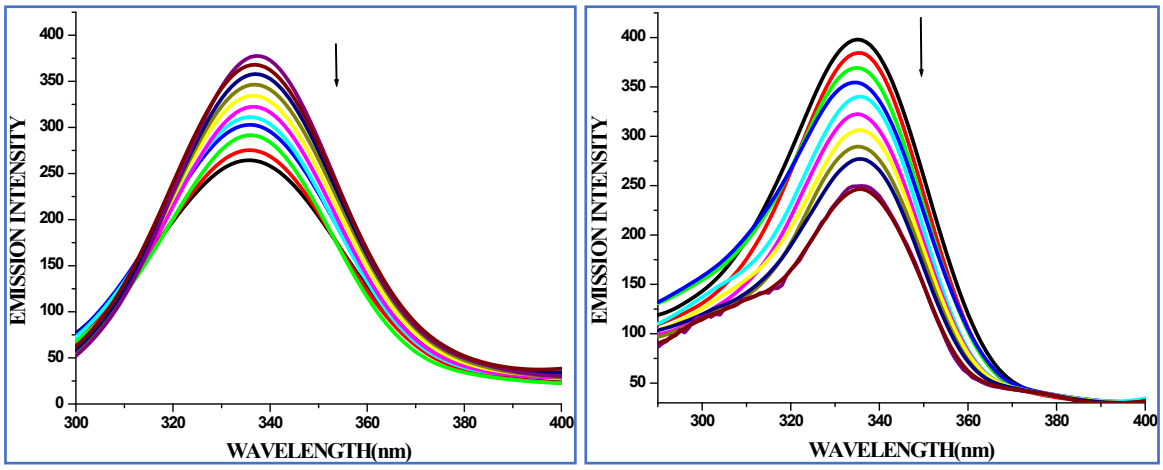


**Fig. S36.** Synchronous spectra of free BSA and BSA (10 μM) in the presence of increasing amounts of ligands (**AQHS$^{1-4}$**) and complexes (**C1-C4**) (10-100) μM concentration for wavelength difference of $\Delta\lambda$ = 60 nm.

**Table S1** Quantum yield data of complexes (**C1-C4**) Shift this to supporting information

| **Complexes** | **$\lambda_{max}$[a] (nm)** | **$\lambda_f$[b] (nm)** | **Stokes shift** | **OD[c]** | **$\phi$[d]** |
|---|---|---|---|---|---|
| **C1** | 325 | 385 | 60 | 0.54 | 0.2151 |
| **C2** | 330 | 383 | 53 | 0.46 | 0.2706 |
| **C3** | 317 | 384 | 67 | 0.56 | 0.2112 |
| **C4** | 323 | 383 | 60 | 0.49 | 0.2867 |

[a]-Absorption maxima. [b]-Maximum emission wavelength. [c]-Optical density. [d]-Quantum yield.

**Table S2** Crystallographic data of ligands **AQHS[1-3]**

| **Compound** | **AQHS[1]** | **AQHS[2]** | **AQHS[3]** |
|---|---|---|---|
| Empirical formula | $C_{17}H_{12}N_6O$ | $C_{18}H_{14}N_6O$ | $C_{18}H_{14}N_6O$ |
| Formula weight | 316 | 330 | 330 |
| Temperature(K) | 298 | 298 | 295 |
| Wavelength(Å) | 1.54184 | 0.71073 | 1.54184 |
| Crystal system | Monoclinic | Monoclinic | Monoclinic |
| Space group | C 1 C 1 | C 1 C 1 | P 1 21/c 1 |
| a (Å) | 11.1604(4) | 12.3680(10) | 15.4757(3) |
| b (Å) | 10.9530(3) | 9.5721(7) | 7.2530(17) |
| c (Å) | 24.0390(7) | 27.193(3) | 14.7604(3) |
| α (°) | 90 | 90 | 90 |
| β (°) | 93.217(3) | 95.157(8) | 99.521(2) |
| γ (°) | 90 | 90 | 90 |
| Volume ($Å^3$) | 2933.89(16) | 3206.3(5) | 1633.98(6) |
| Z | 8 | 4 | 4 |
| Calculated crystal density ($g/cm^3$) | 1.432 | 1.375 | 1.343 |
| Absorption co-efficient ($mm^{-1}$) | 0.785 | 0.092 | 0.727 |
| F(000) | 1312 | 1376 | 688 |
| Crystal size | 0.122x0.096x0.078 | 0.32x0.25x0.18 | 0.5x0.16x0.1 |
| Theta range for data collection (°) | 3.683 to 67.684 | 3.308 to 25.026 | 5.798 to 67.684 |
| Index ranges | -13≤h≤13,<br>-13≤k≤13,<br>-29≤l≤-25 | -14≤h≤14,<br>-11≤k≤11,<br>-32≤l≤32 | -14≤h≤19,<br>-8≤k≤8,<br>-18≤l≤14 |
| Reflections collected/unique | 5175/3963 | 13053/4997 | 13472/3174 |
| Completeness to theta | 99.5 % | 99.8 % | 99.8 % |
| Data/restraints/parameters | 3963/2/436 | 4997/2/455 | 3174/0/229 |
| Absorption correction | Multi-scan | Multi-scan | Multi-scan |
| Max. and min. transmission | 1.00000-0.36621 | 1.00000-0.65393 | 1.00000-0.83489 |
| Goodness-of-fit on $F^2$ | 1.052 | 1.075 | 1.035 |
| Refinement method | Full-matrix least-squares on $F^2$ | Full-matrix least-squares on $F^2$ | Full-matrix least-squares on $F^2$ |
| Final R indices [I > 2sigma(I)] | R1 = 0.0958<br>wR2 = 0.2451 | R1 = 0.0927<br>wR2 = 0.2298 | R1 = 0.0386<br>wR2 = 0.1137 |
| R indices (all data) | R1 = 0.1093<br>wR2 = 0.2614 | R1 = 0.1178<br>wR2 = 0.2641 | R1 = 0.0419<br>wR2 = 0.1184 |
| Largest difference peak and hole ($e/Å^3$) | 0.803 and -0.342 | 0.565 and -0.276 | 0.176and-0.134 |

**Table S3** Selected bond lengths (Å) for ligands **AQHS[1-3]**.

| **AQHS** | | **AQHS[2]** | | **AQHS[3]** | |
|---|---|---|---|---|---|
| N4A-N3A | 1.352(12) | N4A-N3A | 1.360(10) | N1-N2 | 1.3530(16) |
| N4A-N5A | 1.299(13) | N3B-N4B | 1.340(11) | N2-N3 | 1.2954(16) |
| N4A-N5A | 1.299(13) | N6B-N5B | 1.403(9) | N3-N4 | 1.3605(13) |
| N4A-N3A | 1.352(12) | N5A-N6A | 1.390(9) | N5-N6 | 1.3971(13) |
| N4B-N5B | 1.286(14) | N1A-N2A | 1.354(8) | N5-C1 | 1.2630(16) |
| N3B-N4B | 1.358(12) | N2A-N3A | 1.324(11) | N6-C12 | 1.2794(16) |
| N2B-N1B | 1.415(12) | N1B-N2B | 1.371(8) | N1-C10 | 1.3258(15) |
| N5A-N6A | 1.337(12) | N3B-N2B | 1.312(11) | N4-C9 | 1.3913(15) |
| N6B-N5B | 1.381(12) | N1A-C5A | 1.380(10) | N4-C10 | 1.3499(15) |
| N1A-N2A | 1.397(12) | N1B-C5B | 1.378(10) | O1-C18 | 1.3462 |
| N3A-C17A | 1.358(12) | N1A-C10A | 1.358(9) | | |
| N1A-C7A | 1.329(16) | N1B-C10B | 1.362(10) | | |
| N3B-C17B | 1.342(12) | N4A-C10A | 1.323(10) | | |
| N3B-C16B | 1.391(13) | N5A-C11A | 1.225(9) | | |
| N3A-C16A | 1.398(14) | N6A-C12A | 1.307(10) | | |
| N2B-C8B | 1.280(14) | N6B-C12B | 1.291(9) | | |
| O1B-C1B | 1.333(13) | O1A-C14A | 1.351(10) | | |
| O1A-C1A | 1.391(13) | O1B-C14B | 1.352(9) | | |
| C17-N6A | 1.308(13) | C11B-N5B | 1.291(9) | | |
| N6B-C17B | 1.351(13) | C10B-N4B | 1.339(11) | | |
| N2A-C8A | 1.243(15) | | | | |
| N1B-C7B | 1.321(14) | | | | |

**Table S4** Selected bond lengths (Å) and angles (°) for complexes **C1-C4**.

| **Complex C1** | | **Complex C2** | | **Complex C3** | **Complex C4** |
|---|---|---|---|---|---|
| Ru1-Cl04 | 2.4019(17) | Ru1-Cl1 | 2.4010(13) | 2.4152(18) | 2.3999(7) |
| Ru1-N20A | 2.164(5) | Ru1-N1 | 2.057(3) | 2.083(5) | 2.077(2) |
| Ru1-N32A | 2.092(5) | Ru1-N5 | 2.142(3) | 2.156(5) | 2.146(2) |
| Ru1-C1A | 2.225(6) | Ru1-C19 | 2.208(4) | 2.223(7) | 2.206(3) . |
| Ru1-C2A | 2.163(7) | Ru1-C20 | 2.191(4) | 2.198(6) | 2.172(3) |
| Ru1-C3A | 2.214(7) | Ru1-C21 | 2.193(4) | 2.195(7) | 2.185(3) |
| Ru1-C4A | 2.252(6) | Ru1-C22 | 2.216(4) | 2.227(6) | 2.210(3) |
| Ru1-C5A | 2.205(6) | Ru1-C23 | 2.189(4) | 2.202(7) | 2.197(3) |
| Ru1-C6A | 2.194(6) | Ru1-C24 | 2.172(4) | 2.195(7) | 2.202(3) |
| **Complex C1** | | **Complex C2** | | **Complex C3** | **Complex C4** |
| N20A-Ru1-Cl04 | 84.24(14) | N1-Ru1-Cl1 | 83.99(10) | 84.02(17) | 85.37(6) |
| N32A-Ru1-N20A | 84.57(19) | N1-Ru1-N5 | 85.60(12) | 86.55(19) | 85.94(8) |
| N20A-Ru1-C6A | 140.7(2) | N1-Ru1-C19 | 112.97(15) | 115.1(3) | 114.07(10) |
| N20A-Ru1-C5A | 106.8(2) | N1-Ru1-C20 | 94.18(14) | 90.4(3) | 89.73(10) |
| N20A-Ru1-C4A | 91.2(2) | N1-Ru1-C21 | 89.85(14) | 93.1(3) | 92.31(10) |
| N20A-Ru1-C3A | 103.0(3) | N1-Ru1-C22 | 122.06(15) | 120.1(3) | 119.82(11) |
| N20A-Ru1-C1A | 171.2(2) | N1-Ru1-C23 | 159.59(15) | 157.5(3) | 157.33(11) |
| N20A-Ru1-C2A | 135.8(3) | N1-Ru1-C24 | 150.23(16) | 152.8(3) | 151.64(10) |
| N32A-Ru1-Cl04 | 84.51(16) | N5-Ru1-Cl1 | 84.81(9) | 85.43(15) | 85.08(6) |

**Table S5** Hydrogen Bonds for ligands **AQHS[1-3]**(Å and °)

| **AQHS[1]** | | | | |
|---|---|---|---|---|
| **D—H···A** | **d(D—H)** | **d(H···A)** | **d(D···A)** | **∟(DHA)** |
| **N(1A)-H···O(1A)** | 2.027 | 0.820 | 2.668 | 134.59 |
| **N(1B)-H···O(1B)** | 1.947 | 0.820 | 2.656 | 144.13 |
| **Symmetry operations: 'x, y, z', 'x, -y, z+1/2', 'x+1/2, y+1/2, z', 'x+1/2, -y+1/2, z+1/2'** | | | | |
| **AQHS[2]** | | | | |

| **D—H···A** | **d(D—H)** | **d(H···A)** | **d(D···A)** | **∟(DHA)** |
|---|---|---|---|---|
| **N(6A)-H···O(1A)** | 1.966 | 0.821 | 2.628 | 137.15 |
| **N(6B)-H···O(1B)** | 1.907 | 0.819 | 2.613 | 143.77 |
| **Symmetry operations: 'x, y, z', 'x, -y, z+1/2', 'x+1/2, y+1/2, z', 'x+1/2, -y+1/2, z+1/2'** | | | | |
| **AQHS[3]** | | | | |
| **D—H···A** | **d(D—H)** | **d(H···A)** | **d(D···A)** | **∟(DHA)** |
| **N(6)-H···O(1)** | 1.905 | 0.820 | 2.629 | 146.59 |
| **Symmetry operations: 'x, y, z', '-x, y+1/2, -z+1/2', '-x, -y, -z', 'x, -y-1/2, z-1/2'** | | | | |

**Table S6** Hydrogen Bonds for complexes **C1-C4** (Å and °)

| **Complex C1** | | | | |
|---|---|---|---|---|
| **D—H···A** | **d(D—H)** | **d(H···A)** | **d(D···A)** | **∟(DHA)** |
| **N(19A)-H···O(11A)** | 1.925 | 0.820 | 2.635 | 144.31 |
| **Symmetry operations:** 'x, y, z', '-x, -y, -z' | | | | |
| **Complex C2** | | | | |
| **D—H···A** | **d(D—H)** | **d(H···A)** | **d(D···A)** | **∟(DHA)** |
| **N(6)-H···O(1)** | 1.902 | 0.820 | 2.615 | 144.75 |
| **Complex C3** | | | | |
| **D—H···A** | **d(D—H)** | **d(H···A)** | **d(D···A)** | **∟(DHA)** |
| **N(6)-H···O(1)** | 1.961 | 0.820 | 2.649 | 140.95 |
| **Symmetry operations:** 'x, y, z', '-x, y+1/2, -z+1/2', '-x, -y, -z', 'x, -y-1/2, z-1/2' | | | | |
| **Complex C4** | | | | |
| **D—H···A** | **d(D—H)** | **d(H···A)** | **d(D···A)** | **∟(DHA)** |
| **N(6)-H···O(1)** | 1.895 | 0.820 | 2.612 | 145.45 |
| **Symmetry operations:** 'x, y, z', '-x, y+1/2, -z+1/2', '-x, -y, -z', 'x, -y-1/2, z-1/2' | | | | |

| LIGANDS | LIGAND REDUCTION | | | | LIGAND OXIDATION | | | |
|---|---|---|---|---|---|---|---|---|
| | $Ep_a$ (V) | $Ep_c$ (V) | $E_{1/2}$ (V) | ΔEp (mV) | $Ep_a$ (V) | $Ep_c$ (V) | $E_{1/2}$ (V) | ΔEp (mV) |
| **AQHS[1]** | -1.516<br>-0.927 | -1.636<br>-1.217 | 1.576<br>1.022 | 120<br>290 | 0.301 | -0.167 | 0.234 | 468 |
| **AQHS[2]** | -1.542<br>-0.946 | -1.664<br>-1.194 | 1.603<br>1.07 | 122<br>248 | 0.269 | -0.144 | 0.206 | 413 |
| **AQHS[3]** | -0.918 | -1.244 | 1.081 | 326 | 0.370 | -0.087 | 0.228 | 457 |
| **AQHS[4]** | -1.569<br>-1.001 | -1.705<br>-1.258 | 1.637<br>1.120 | 136<br>257 | 0.296 | -0.087 | 0.190 | 383 |

**Table S7** Electrochemical data for ligands

**Table S8** The binding constant ($K_{bin}$) and quenching constant ($K_{sv}$) values for the interactions of the ligands and the complexes with CT-DNA.

| Compounds | Binding constant $K_{bin}$ $M^{-1}$ | Quenching constant $K_{SV}$ $M^{-1}$ | $K_{app}(M^{-1})$ |
|---|---|---|---|
| **AQHS[1]** | 3.28 x$10^4$ | 5.02 x$10^3$ | 1.33 x$10^6$ |
| **AQHS[2]** | 8.77 x$10^4$ | 4.43 x$10^3$ | 1.40 x$10^6$ |
| **AQHS[3]** | 1.51 x$10^5$ | 4.72 x$10^3$ | 1.56 x$10^6$ |
| **AQHS[4]** | 1.18 x$10^4$ | 5.06 x$10^3$ | 1.61 x$10^6$ |
| **C1** | 3.01 x$10^5$ | 5.82 x$10^3$ | 1.78 x$10^6$ |
| **C2** | 1.65 x$10^5$ | 5.29 x$10^3$ | 1.72 x$10^6$ |
| **C3** | 2.83 x$10^5$ | 6.01 x$10^3$ | 1.85x$10^6$ |
| **C4** | 3.15 x$10^5$ | 9.96 x$10^3$ | 1.92 x$10^6$ |

**REFERENCES**


1. Vogel, A.I. "*Textbook of practical organic chemistry*, 5th Ed., Longman, London. 1989, 268.
2. Bekhit, A.A.; El-Sayed, O.A.; Aboulmagd, E; Park, J.Y. Tetrazolo [1, 5-a] quinoline as a potential promising new scaffold for the synthesis of novel anti-inflammatory and antibacterial agents. *Eur. J.Med. chem.* 2004, *39*(3), 249-255.
3. Nippu, B.N.; Rahman, A.; Kumaraswamy, H.M.; Satyanarayan, N.D. Design and synthesis of novel tetrazolo quinoline bridged isatin derivatives as potential anticancer leads against MIA PaCa-2 human pancreatic cancer cell line. *J. Mol. Struct.* 2022, *1263*, 133103.
4. Rose, B.J.; Ranjani, M.; Kalaivani, P.; Prabusankar, G.; Kaminsky, W.; Prabhakaran, R. Novel 5-(2-chloro-quinolin-3-yl)-[1, 3, 4] thiadiazol-2-ylamines and their copper (II) metallates: Preparation, spectroscopy, X-ray crystallography, nucleic acid/albumin binding, DNA cleavage and in vitro cytotoxicity. *Inorg. Chim. Acta.* 2024, *570*, 122170.
5. Sindhu, M.; Kalaivani, P.; Prabusankar, G.; Sivasamy, R.; Prabhakaran, R. Preparation of new organo-ruthenium (II) complexes and their nucleic acid/albumin binding efficiency and in vitro cytotoxicity studies. *Dalton Trans.* 2024, *53*(7), 3075-3096.
6. Passi, I.; Abraham, L.M.; Wilfred Raj, A.S.W.; Varadhan, M.; Muthuraman, S.; Sivaramakrishnan, M.P.; Vadivelu, P.; Manoharan, R.; Velusamy, M.; Rajendiran, V. Enhanced Cytotoxicity of Half-Sandwich Ruthenium (II) Complex Containing Nitro-Substituted Salicyllimidazo [1, 5-a] pyridine toward Hormone-Independent Triple-Negative Breast Cancer Cells. *Inorg. Chem.* 2025, *64*(28), 14073-14090.
7. Ponnusamy, L.; Kothandan, G.; Manoharan, R. Berberine and Emodin abrogates breast cancer growth and facilitates apoptosis through inactivation of SIK3-induced mTOR and Akt signaling pathway. *Biochim. Biophys. Acta - Mol. Basis Dis.* 2020, *1866*(11), 165897.
8. Nandhini, S.; Ranjani, M.; Thiruppathi, G.; Jaithanya, Y.M.; Kalaiarasi, G.; Ravi, M.; Prabusankar, G.; Malecki, J.G.; Sundararaj, P.; Prabhakaran, R. Organoruthenium metallocycle induced mutation in gld-1 tumor suppression gene in JK1466 strain and appreciable lifespan expansion. *J. Inorg. Biochem*. 2024, *257*, 112593.
9. Nandhini, S.; Thiruppathi, G.; Ranjani, M.; Puschmann, H.; Ravi, M.; Sundararaj, P.; Prabhakaran, R. Effect of ruthenium (II) complexes on MDA-MB-231 cells and

lifespan/tumor growth in gld-1mutant, Daf-16 TF and stress productive genes: A perspective study. *J. Inorg. Biochem*. 2024, *257*, 112580.